Effects of dead elements in ultrasound transducers

HELENA GISTVIK

SARA PETTERSSON

KTH Technology and Health

Master of Science Thesis in Medical Engineering

Stockholm 2013

This master thesis project was performed in collaboration with
GE Healthcare
Supervisor at GE Healthcare: Geir Haugen

Effects of dead elements in ultrasound transducers

Effekter av döda element i ultraljudstransducers

HELENA GISTVIK
SARA PETTERSSON

Master of Science Thesis in Medical Engineering
Advanced level (second cycle), 30 credits
Supervisor at KTH: Mattias Mårtensson
Examiner: Lars-Åke Brodin
School of Technology and Health
TRITA-STH. EX 2013:77

Royal Institute of Technology
KTH STH
SE-141 86 Flemingsberg. Sweden
http://www.kth.se/sth

Abstract

Ultrasound is a common modality used in healthcare today. The ultrasound images can be used as a diagnostic tool and the image quality is therefore important. Earlier studies have shown that transducers used clinically are often damaged; a type of damage is dead elements in the transducer. In this study, it has been evaluated how the number and the placement of the dead elements impact the beam profile and how this is reflected in the image quality. This has been performed with two types of simulations, one simulated beam profiles and the other simulated dead elements in a transducer used to create real images. The results showed that the beam profile was affected by both the number and the placement of dead elements. It has not been determined how the altered beam profile affected the image quality, but there were indications that the image quality deteriorated when there were dead elements in the transducer. As both the number of dead elements and their placement affected the beam profile, an acceptance level could not be suggested regarding the number of dead elements.

Sammanfattning

Ultraljud är en vanlig modalitet i dagens sjukvård. Ultraljudsbilderna kan användas som ett diagnostiskt hjälpmedel och bildkvaliteten är därför viktig. Tidigare studier har visat att transducers, som används kliniskt, ofta är skadade och en typ av skada är döda element i transducern. I den här studien undersöktes hur antalet döda element och deras placering påverkar strålprofilen och hur dessa förändringar avspeglas i bildkvaliteten. Detta gjordes med hjälp av två simuleringstyper, den ena simulerade strålprofiler och den andra simulerade döda element i en transducer som användes till att framställa riktiga bilder. Resultaten visade att strålprofilen påverkades av antalet döda element såväl som deras placering. Det kunde inte bestämmas hur den förändrade strålprofilen påverkade bildkvaliteten, men det fanns indikationer som tydde på att bildkvaliteten försämrades av döda element. Eftersom både antalet döda element och deras placering påverkade strålprofilen, kunde inte en acceptansnivå gällande antalet döda element föreslås.

Acknowledgement

This report was written as a part of the course HL202X at the Royal Institute of Technology. It presents the results of a master thesis study in which the effects of dead elements in ultrasound transducers were evaluated. The study was performed in cooperation with General Electric Vingmed Ultrasound (GE) in Oslo, Norway.

We are grateful to everyone who has helped and supported us during the project. We would especially like to thank Mattias Mårtensson, our supervisor at the Royal Institute of Technology, and Geir Haugen, our supervisor at GE.

Table of contents

1. Introduction

Ultrasound is a common modality in modern healthcare, both for diagnostic purposes and for treatment. The most known area of use is foetal monitoring but the technique is also used to image the heart and other soft tissues such as liver and kidneys. Compared to other imaging techniques, ultrasound is cheap and not considered to be harmful since there is no use of ionizing radiation. Ultrasound produces images in real-time, which is another advantage of the technique. An image is obtained by scanning the area of interest with a transducer that consists of piezoelectric elements.

It is known that transducers are sensitive to outer impact and a previous study has shown that transducers used in clinical care are often damaged [1]. In this study, 39.8% of the transducers had some kind of defect. The most common error type was delamination, meaning that the layers in the transducers detach from each other. Approximately four per cent of the evaluated damaged transducers had defective elements, that is, dead or not fully functioning. The cause of damage can be normal wear, quality problems or the human factor.

1.1. Problem definition

To obtain high-quality images with ultrasound, the function of the transducer is the most important component of the equipment [2]. There are transducers with dead elements in use and according to an earlier study as little as two consecutive dead elements in a transducer can significantly alter the beam profile [3]. It is, however, unknown how the location and the number of dead elements affect the beam profile and how the altered beam profile affects image quality. The quality of the ultrasound image is important, as the image can be the basis for a diagnosis.

1.2. Objective

The purpose of this study was to evaluate the effects on beam profiles resulting from dead elements in transducers. It was evaluated how the number of dead elements and their location affected the beam profile and if these effects were reflected in the image quality. This was done by performing and comparing two simulation types, one simulated beam profiles and the other simulated dead elements in a transducer used to create real images. Furthermore, an acceptance level regarding the number of dead elements in ultrasound transducers was discussed.

1.3. Limitations

In this study, only two-dimensional ultrasound with phased array transducers has been considered. No errors except dead elements have been taken into account. The combinatorial possibilities regarding the placement and the number of dead elements are extensive why only a number of error configurations and a limited number of dead elements were considered in this study.

2. Literature study

This chapter aims at giving the reader an introduction of ultrasound and its features for a better understanding of the results of this study. This chapter is based on information from *"Diagnostic Ultrasound – Physics and Equipment"* [4] if nothing else is stated.

2.1. Ultrasound

Ultrasound is sound with a frequency higher than the audible range for humans, that is, higher than 20 kHz. Frequencies between 2 and 15 MHz are most common in medical applications. The areas of use are many, for example, foetal monitoring and imaging of the heart and intestines. With modern ultrasound techniques it is also possible to measure blood flow and tissue velocity. Unlike imaging techniques that use ionizing radiation, for example X-ray and computed tomography, ultrasound exposure is not considered to be harmful. The technique is also cheap compared to other imaging methods, for example magnetic resonance imaging.

During an ultrasound examination, ultrasound is transmitted from the transducer and travels through the tissue until it reaches an interface between two media with different acoustic impedance. The acoustic impedance Z is proportional to the product of the sound velocity c and the tissue density ρ, according to Equation 1.

$$Z = c \cdot \rho$$

Equation 1

In interfaces, the ultrasound wave will be partially reflected and the reflected fraction depends on the acoustic impedance of the materials. A large difference in acoustic impedance results in a larger echo and vice versa. Air has very low acoustic impedance compared to soft tissue, which leads to what is regarded as total reflection and thus tissues behind such an interface cannot be imaged. Bone has high acoustic impedance compared to soft tissue and the reflection is large, which makes it principally impossible to image through it.

The returning echoes are used to create an image. The shade of grey in the image corresponds to the amplitude of the echo. Strong echoes correspond to white in the image, whereas black corresponds to no echo. Ultrasound is attenuated linearly in tissue and, therefore, it is common to compensate for lost energy due to travelled distance. This is done to ensure that echoes from similar interfaces are imaged with equal intensity.

To obtain grey-scale ultrasound images, pulsed wave ultrasound is used and pulses are sent out from the transducer at specific time intervals. The time of one pulse is called pulse length and the time between transmissions of two consecutive pulses is called pulse repetition period, see Figure 1. The pulse travels through tissue and is reflected at interfaces in the line of propagation, as described earlier.

The transducer is acting as both transmitter and receiver. The returning echoes contain information that is used to create the image. The depth of the interfaces can be calculated using the sound velocity and the time travelled.

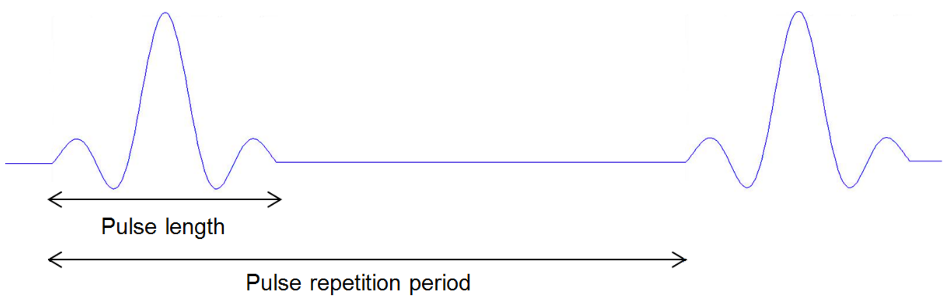

Figure 1. In pulsed wave ultrasound, pulses are sent out with specific time intervals. Pulse repetition period describes the time between the transmissions of two consecutive pulses. The pulse length is the duration time for one pulse. The x-direction represents time.

2.2. The transducer

The transducer is the handhold part of the ultrasound equipment that is in direct contact with the patient. The transducer consists of a group of elements made of a piezoelectric material. This material has the ability to convert electrical energy to mechanical energy and vice versa. When a positive or negative voltage is applied on the polarized piezoelectric material it either compresses or stretches, resulting in the creation of a mechanical wave. When the echo returns, the mechanical energy is converted to an electrical signal which is used to create an image.

The front surface of the piezoelectric elements is covered with one, or more, matching layers. The matching layers have acoustic impedances that are between the impedances of the piezoelectric material and the tissue to optimize transmission between the transducer and the patient. A lens can be attached to the matching layer in order to focus the beam. On the rear side of the piezoelectric elements there is a backing layer. An efficient backing layer stops the vibration of the piezoelectric elements after the electrical pulse, which enables a shorter pulse length. A schematic image of a transducer can be seen in Figure 2.

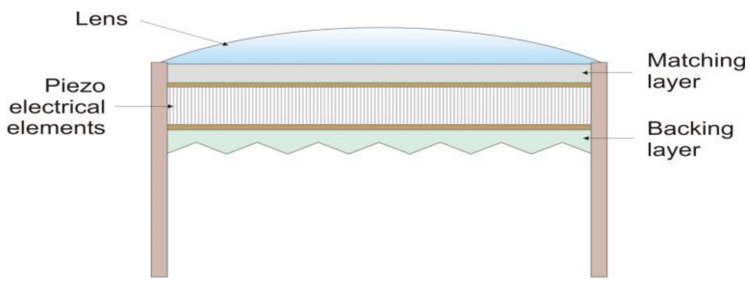

Figure 2. Schematic image of an ultrasound transducer

There are several different types of transducers, optimized for different purposes. Cardiac probes are phased array transducers, they are small to fit between the ribs of the patient and the emitted field has the shape of a sector. By delaying the excitation of certain elements in the transducer, the beam can be directed in different angles and be focused at different depths, see Figure 3. The emitted waves from the elements will interfere and create a wave front. The sector is composed of multiple steered beams, where one beam is referred to as a scan line [5]. To obtain a scan line, all elements in the transducer are activated [6].

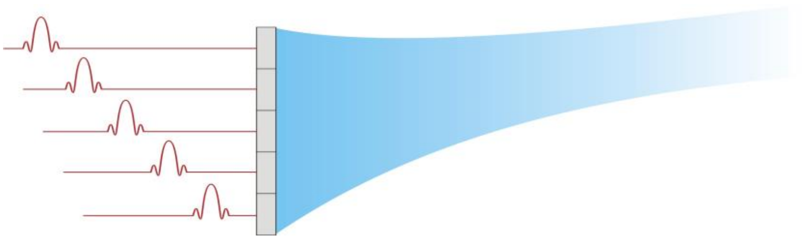

Figure 3. Illustration of beam steering with time delay

The delay of a given element can be calculated by determining the difference in travel time to the desired focus point compared to adjacent elements. By using the distance formula according to Equation 2 and the speed of sound in tissue c, a time-vector can be obtained [7].

$$\bar{t}_{focus} = \sqrt{(\bar{x} - \bar{x}_{focus}) + (\bar{y} - \bar{y}_{focus}) + (\bar{z} - \bar{z}_{focus})}/c$$

Equation 2

2.3. Resolution

The image quality depends on the spatial and the contrast resolution [8]. The spatial resolution of an ultrasound image is divided into axial, lateral and elevational resolution [9]. Axial resolution is the ability to distinguish between two reflectors in the axis along the ultrasound beam, whereas lateral resolution is the ability to dissolve two reflectors perpendicular to the direction of travel, see Figure 4.

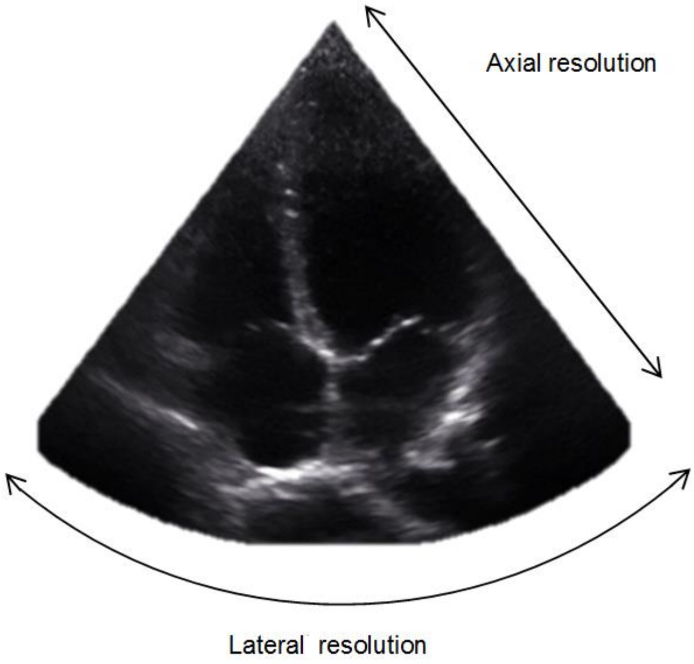

Figure 4. Four chamber view of the heart with the lateral and axial directions marked. Courtesy of Britta Lind, STH, KTH.

The axial resolution depends on the features of the pulse. A shorter pulse length, which can be obtained by increasing the frequency or limit the number of cycles in the pulse, results in better axial resolution. Higher frequencies are, however, absorbed faster and the penetration depth is therefore reduced.

The lateral resolution depends on the width of the beam. A narrow beam yields better lateral resolution. The lateral resolution also depends on the depth of imaging as the beam widens when it penetrates deeper into the tissue. For better lateral resolution, the beam is focused.

Contrast resolution describes the ability of the equipment to detect small differences in acoustic impedance.

2.4. Beam profile

One way to evaluate the performance of an ultrasound transducer is to assess the features of the beam profile. The assessment is normally done on a plot of the intensity or pressure measured in decibel as a function of lateral distance from the transducer centre. The narrow peak, in Figure 5, is referred to as the main lobe or main peak and the lowest level is referred to as the noise floor. Due to interference, weaker lobes can appear on the sides of the main lobe. These are called side lobes and can be visualised in the plot of the broken transducer. The main lobe should have a higher intensity compared to the side lobes.

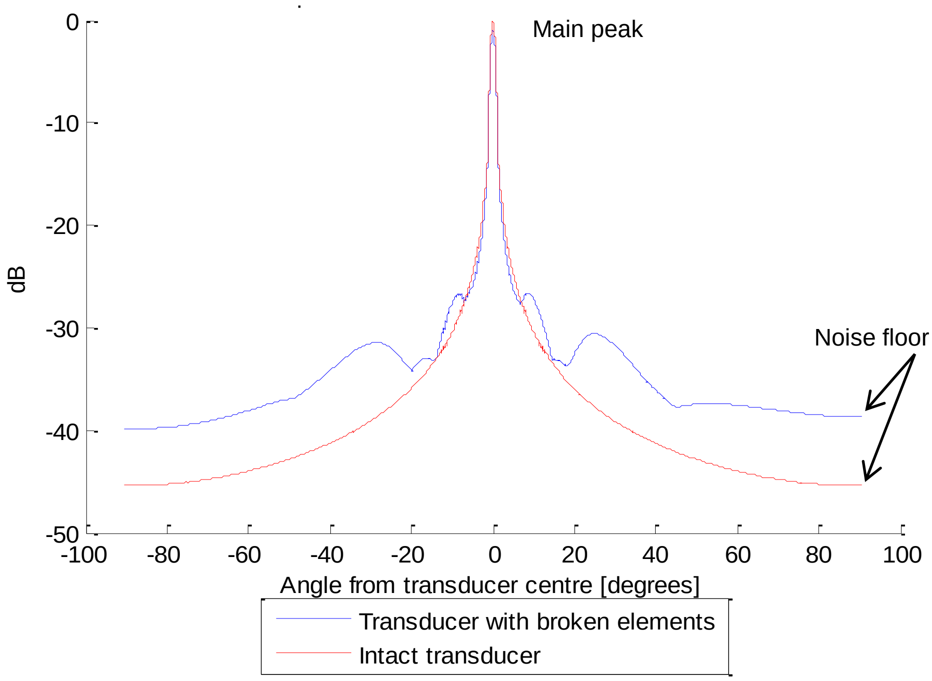

Figure 5. Beam profiles of intact transducer and transducer with dead elements.

A special case of side lobes is grating lobes. While side lobes are directed forward, grating lobes are directed away from the main beam with a large angle, see Figure 6 [6]. Side lobes and grating lobes can give rise to artefacts [6]. In ultrasound, echoes are assumed to return from the main beam, this is, however, not always the case when side lobes are present. Resultantly, an echo obtained from a side lobe appears in the image as if it was located in the line of travel of the main beam.

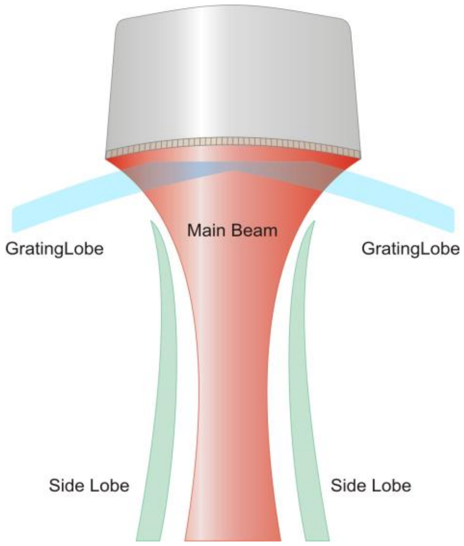

Figure 6. Illustrative image of grating and side lobes

The -6 dB beam width is a measure of the function of the transducer. This is the point at which the intensity is half of the maximum intensity, see Equation 3. This is often referred to as the full width at half maximum (FWHM). It can also be regarded as the lateral resolution [10].

$$Beam\ width = 20 \cdot \log \frac{0.5P_0}{P_0} = -6\ dB$$

Equation 3

2.5. Image representation

The rendering of an object in ultrasound imaging can be described by Equation 4 [11].

$$g(r) = \int f(\tau) \cdot h(r - \tau)\ d\tau$$

Equation 4

The actual object f is convolved, with the impulse response h of the equipment to obtain the image $g(r)$. The position of g is given by r in spatial coordinates. The impulse response of the equipment, sometimes called the point spread function, will spread out the object and consequently, creating a smeared image, see Figure 7. Dead elements in a transducer alter the impulse response of the equipment which affects the image of the object.

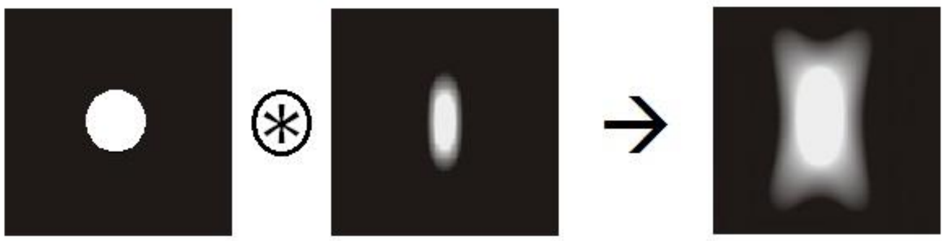

Figure 7. Illustrative description of image rendering, the left image represents the actual object, the middle the impulse response and the right the resulting image of the object.

Mathematically, the convolution of two functions can be seen as the common area under the two graphs for each τ [12]. In this case, the shared area under f and h are added for each τ, which results in a function g that is a modified version of f.

2.6. Testing of transducers

Equipment used for ultrasound examinations need to be tested on regular basis to ensure secure functioning. There are different test procedures depending on what function of the equipment that is to be evaluated. A two-dimensional test phantom consists of a box filled with a material in which the speed of sound resembles that of soft tissue. To this material a fine ground powder, for example graphite, is added to obtain the speckle pattern that is present in ultrasound images. Inside the phantom there are targets for measuring parameters of image quality. The targets have acoustic impedances that differ from the soft tissue and they are placed on different depths and lateral positions in the phantom. Figure 8 displays an ultrasound image of a two-dimensional phantom, where a round black cyst can be visualised in the upper left part of the image and point spreaders as the white dots in straight lines.

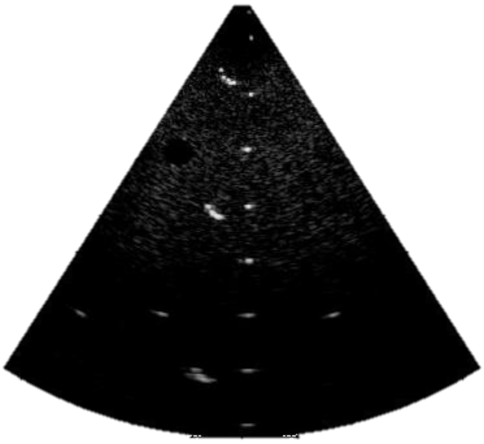

Figure 8. Ultrasound image of a two-dimensional phantom, a cyst can be visualised to the left and point spreaders as the white dots in straight lines.

2.7. Image quality assessment

The quality of an ultrasound image is important as the image can be the basis for a diagnosis. There are two ways to evaluate image quality: subjective and objective image quality assessment [13, 14]. Subjective image quality assessment is done by an individual who, for example, evaluates the image quality of a standardized phantom by ocular inspection. Objective image quality assessment is done by evaluating different measured values of an image, such as signal to noise ratio (SNR) and mean square error (MSE) [13, 14].

The advantage of using objective assessment is that it enables quick evaluation of data and yields results that are comparable to each other. However, objective quality assessment does not always coincide with the human perception of an image, which subjective image quality assessment does [13, 14].

2.8. Earlier studies regarding effects of dead elements

There are few studies regarding how dead elements in ultrasound transducers affect the image quality of the system. However, one study showed that two dead elements in a 128-element transducer resulted in increased side-lobe levels and four dead elements reduced the main peak intensity [3]. Two dead elements is also the criterion of a defective transducer at Karolinska University Hospital in Stockholm, Sweden [1]. It has been shown that a reduction in peak intensity can lead to lower penetration depth [3]. Consequently, the optimal depth of imaging stated by the manufacturers will no longer be valid. An intensity loss and an increase of side-lobe level can result in reduced lateral and contrast resolution.

3. Method

The simulations were made using *Field II Simulation Program 3.20b* (Field II), an ultrasound simulation programme, developed by Jørgen Arendt Jensen at the Technical University of Denmark [2, 15] and *Matlab R2012a* (Mathworks Inc. Natick, MA, USA).

3.1. Field II simulations

Field II consists of a number of Matlab-functions that calls a programme in C, which performs calculations regarding the emitted ultrasound field [16].

A Field II programme that simulated one intact and ten broken transducers was constructed, see Appendix 1. Each transducer consisted of 96 piezoelectric elements in one row. One transducer was fully functional while the others had a predefined number of dead elements, spread over the surface, see example in Figure 9.

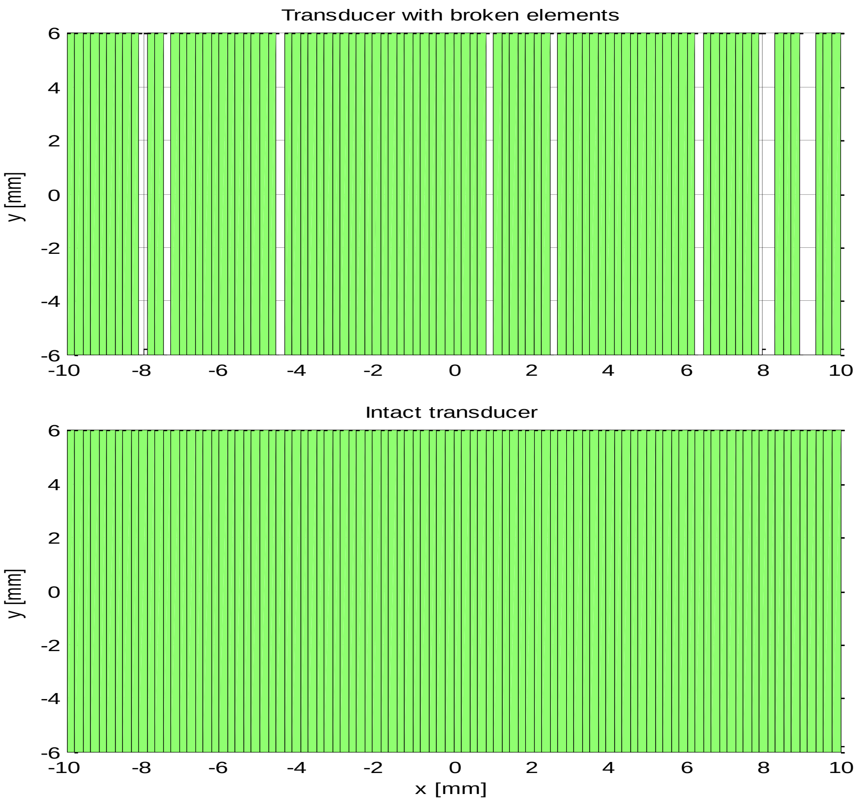

Figure 9. Surfaces of a transducer with broken elements, in the topmost picture, and of an intact transducer in the lower

The total width of the piezoelectric elements was 20 mm, which is approximately the same size as the transducer used to collect data to Test II, see section 3.2. There were gaps between the elements called kerfs, and each gap was one tenth of the element width. The elements were excited and the pressure field was determined in points at a radius of 7.76 cm from the transducer surface. The focus depth was also set to 7.76 cm. This depth was chosen as the same depth that was used in Test II. The pressure field was plotted in decibels, as a function of angle from the transducer centre. The beam profiles of the broken transducers were normalised to 0 dB.

The used transmission frequency was 3 MHz and the sampling frequency was 100 MHz. The velocity of sound was assumed to be 1 540 m/s in the medium of travel and the attenuation was set to 0.5 dB/(MHz·cm).

For a focused transducer, the approximate beam width in the focal region is described by Equation 5 [5, 8]. To ensure the credibility of the simulation, this was tested.

$$Beam\ width_{-3\ dB} = \frac{focal\ length}{diameter} \cdot \lambda$$

Equation 5

A plot of the pressure field for an intact transducer in Field II is shown in Figure 10.

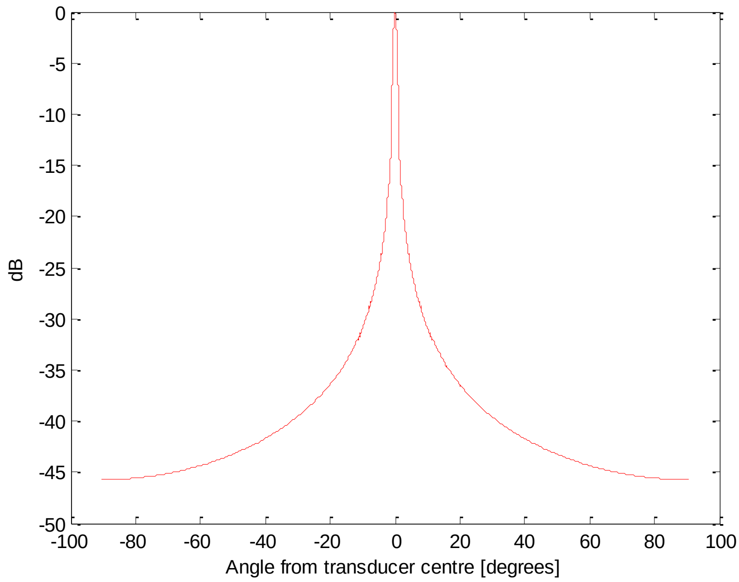

Figure 10. Beam profile for the intact transducer

3.2. Real-data simulation

Real images were collected with a Vivid E9 machine and a M5S-D transducer, both manufactured by GE, on a two-dimensional phantom (Gammex RMI 403GS). All elements of the transducer were excited and the beam was focused in zero degrees. Reception was carried out with one element at the time, which resulted in the collection of 192 files, each corresponding to an image. In this study, consideration has only been taken to the middle row of the transducer.

Code obtained from GE was altered to fit the needs of this study. It was used to read the files and summarise the image information in order to obtain a total image. To simulate dead elements, the corresponding files were not added to the total image. Thereafter, the total image was imported into a second programme made, as a summer project at GE, by Julia B. Jørgensen. This code was also altered to fit this study. This programme consisted of several functions that analysed the image and yielded plots that visualised the axial and lateral resolution of the point spreaders and the cysts in the phantom. In this study, the point spreader at a depth of 7.76 cm and the cyst at a depth of 5.81 cm were analysed.

3.3. Test procedure

Test I

Field II simulations were done for different types of error configurations, see Table 1. Every test was performed with ten different sets of dead elements. The choice of elements is further described in chapter 3.3.1 and all error patterns are presented in Appendix 2. The beam was focused to zero degrees, which is perpendicular to the transducer surface. Additionally, the same error patterns were simulated with steering angles twenty and forty degrees respectively.

Table 1. Test description.

Number of dead elements	Random	Grouped	Edge
5	X	X	X
10	X	X	X
15	X	X	-
20	X	X	-
30	X	X	-

In the simulations, information about the locations of the dead elements, the beam width in -3 dB and -6 dB, as well as the pressure loss of the main peak for the broken transducer was collected in a Microsoft Excel file (Microsoft Office, version 2010, Redmond, WA, USA). The average side-lobe level was determined by selecting the highest side lobe on each side of the main lobe and the mean value was calculated. In the cases where no side lobes were obtained, the mean of the configuration was taken only for those error patterns where side lobes were present. In this study, no difference was made between side lobes and grating lobes. The noise floor of each error pattern was chosen as the higher of the two end points in the corresponding plot.

Test II

All error patterns were run through the real-data simulation and intensity profiles were plotted, see Figure 11. Information regarding resolution was obtained by measuring the distances between two points of intensity -6 dB and -12 dB on each side of the peak value.

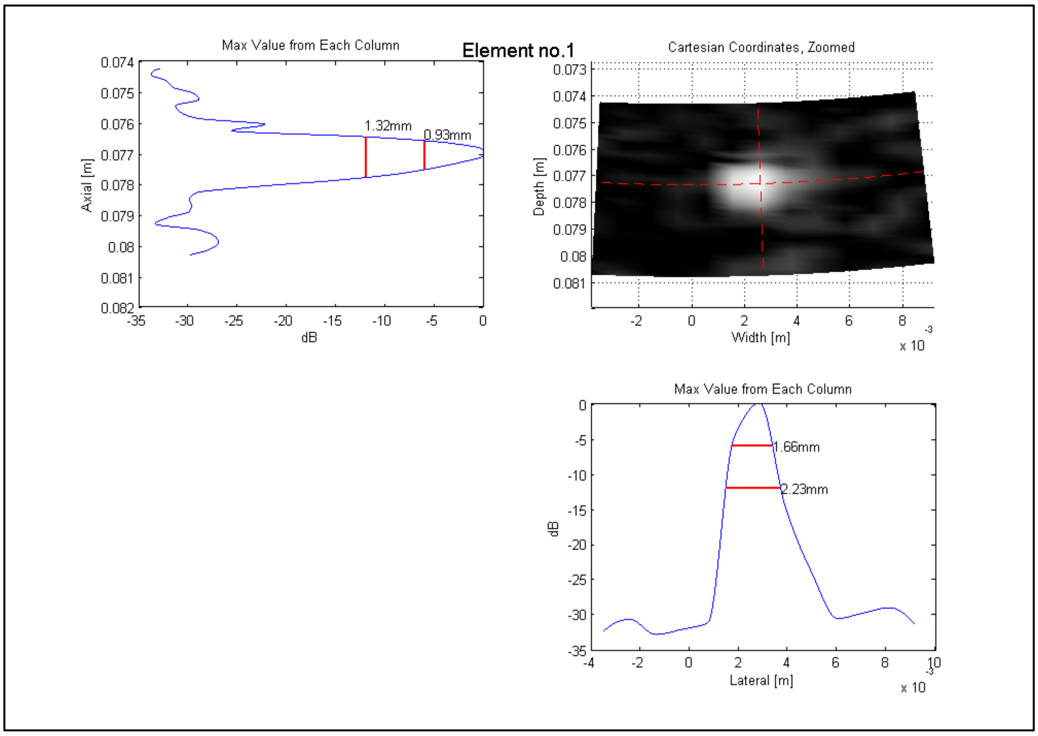

Figure 11. Analysis of a point spreader. The top left plot describes the intensity in the point spreader for the axial direction, the top right picture displays the image of the point spreader from the ultrasound image and the bottom panel shows the intensity of the point spreader in the lateral direction. The plots are obtained from the intensity values of the pixels corresponding to the red lines in the upper right picture.

The percentage intensity losses were calculated by determining the maximum intensity in the point spreader for the intact transducer and the transducer with dead elements. The SNR was determined by the obtained code. It was calculated by determining the intensity of points in the point spreader respectively outside the point spreader. All values were gathered in a Microsoft Excel file.

3.3.1. Choice of dead elements

The dead elements were randomly chosen with the predefined function *randi* in Matlab. The function returned a random integer value from a uniform distribution of specified values, in this case 1-96, which corresponded to the indices of the elements.

First, one test-set consisting of ten different random error patterns was made. Each error pattern consisted of n = {5, 10, 15, 20, 30} unique dead elements. Second, the dead elements were forced into groups. This was done by dividing the *n* dead elements into groups of varied and randomised size. One group consisted of one to *n* consecutive dead elements. The start index for each group was also randomised using *randi*. In a third step, the dead elements were forced to the edges of the transducer. *Randi* was used to determine how many of the *n* dead elements that were placed at the left side of the transducer, the remainder were placed at the right side.

3.4. Comparison of results

The percentage loss of intensity obtained from the two simulation types was compared as they were considered to be equivalent.

The noise floor was compared to the SNR with reference to behaviour when the number of dead elements and their location changed.

The beam width in -3 dB from Test I was compared to the -6 dB width in Test II. In Test II, the ultrasound had travelled to a depth of 7.76 cm and back to the transducer before measurements were done, yielding a total travelled distance of 15.52 cm, that is, twice as far as in Test I. Attenuation of ultrasound, measured in decibel, is linear in tissue and therefore, the -3 dB beam width in Test I corresponded to the -6 dB width in Test II. If not specified, the values given in this report are round-trip measures.

As side lobes distribute energy in other directions than the main beam, the average side-lobe level was compared to the change of intensity in the cyst, which was located outside the main beam.

4. Results

Tables of results from Test I can be found in Appendix 3, 4, and 5, and the results from Test II can be found in Appendix 6.

4.1. Test I

The following section presents the results from the Field II simulations. Results that were general for all steering angles are presented first, and thereafter the specific results for each steering angle. The results are given as the mean value ± two standard deviations for each error configuration. The standard deviations were consistently high with exception to the loss of intensity, in which the standard deviations were close to zero.

In Test I, the loss of intensity in the main peak followed the number of dead elements, see Table 2. The intensity loss was equal for all steering angles and the location of the dead elements did not affect the result.

Table 2. The remaining intensity in the main beam was unaffected by steering.

Number of dead elements	Random [%]	Grouped [%]	Edge [%]
5	94.8 ± 0.0	94.8 ± 0.0	94.8 ± 0.0
10	89.5 ± 0.0	89.2 ± 0.0	89.6 ± 0.0
15	84.4 ± 0.0	84.4 ± 0.0	-
20	79.2 ± 0.0	79.2 ± 0.0	-
30	68.7 ± 0.0	68.6 ± 0.0	-

The average beam width in -3 dB (one-way), corresponding to lateral resolution, was not affected by the number of dead elements for the randomised and grouped configurations. The location of the dead elements, however, affected the beam width. For example, the range in beam width for thirty grouped dead elements was 1.47 mm to 2.06 mm when the beam was directed to zero degrees. Dead elements only at the edges of the transducer yielded wider beam-widths than the other two configurations and the standard deviations were lower. In this case, the beam width was slightly wider for ten dead elements than for five dead elements.

The width of the beam increased with steering, the intact transducer had a width of 1.67 mm for zero degree steering, and 1.79 and 2.20 mm respectively for twenty and forty degree steering. The beam width of the broken transducers widened when the beam width of the intact transducer did.

Beam profiles from transducers in which all dead elements were in one group, and from transducers with dead elements only at the edges, had appearances that differed from the other beam profiles. Error patterns where all elements were in one group had curves that followed the curve of the intact transducer for high and low decibel values, but were wider for intermediate values, see Figure 12a. Transducers that had dead elements only at the edges had beam profiles that were a bit wider than that of the intact transducer, see Figure 12b. This was consistent for all steering angles.

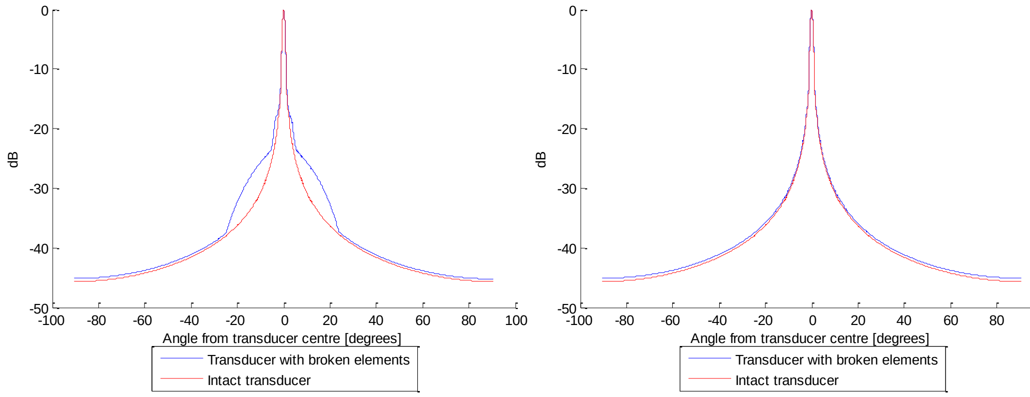

Figure 12. a) Beam profile of transducer with all dead elements in one group. b) Beam profile of transducer with dead elements only at the edges.

4.1.1. Zero degrees steering

The noise floor increased with the number of dead elements. The increase was higher for random dead elements but the standard deviations were, however, higher for grouped dead elements. In comparison, dead elements at the edges of the transducer resulted in a smaller increase of the noise-floor level with smaller standard deviations than the other two error configurations, see Table 3.

Table 3. Increase of noise floor compared to the intact transducer, which has a noise floor level of -45.6 dB.

Number of dead elements	Random [ΔdB]	Grouped [ΔdB]	Edge [ΔdB]
5	6.30 ± 1.38	3.94 ± 5.16	0.55 ± 0.10
10	7.65 ± 1.34	3.96 ± 5.36	1.09 ± 0.20
15	8.59 ± 0.80	4.88 ± 4.78	-
20	9.40 ± 0.72	5.22 ± 5.50	-
30	10.9 ± 0.70	8.22 ± 4.40	-

The average side-lobe level increased with the number of dead elements, see Table 4. Grouped dead elements yielded higher average values. For the two cases where dead elements were at the edges, no side lobes were obtained and therefore no values are presented.

Table 4. Average side-lobe level.

Number of dead elements	Random [dB]	Grouped [dB]
5	-33.1 ± 3.98	-20.0 ± 9.20
10	-26.1 ± 9.34	-18.9 ± 9.26
15	-25.6 ± 7.42	-15.1 ± 5.24
20	-22.9 ± 9.92	-15.2 ± 7.20
30	-21.3 ± 9.72	-12.7 ± 6.24

4.1.2. Twenty degree steering

The beam profile of the intact transducer, steered to twenty degrees, is presented in Figure 13. The beam profile has an increased noise floor on the right side compared to the transducer steered to zero degrees.

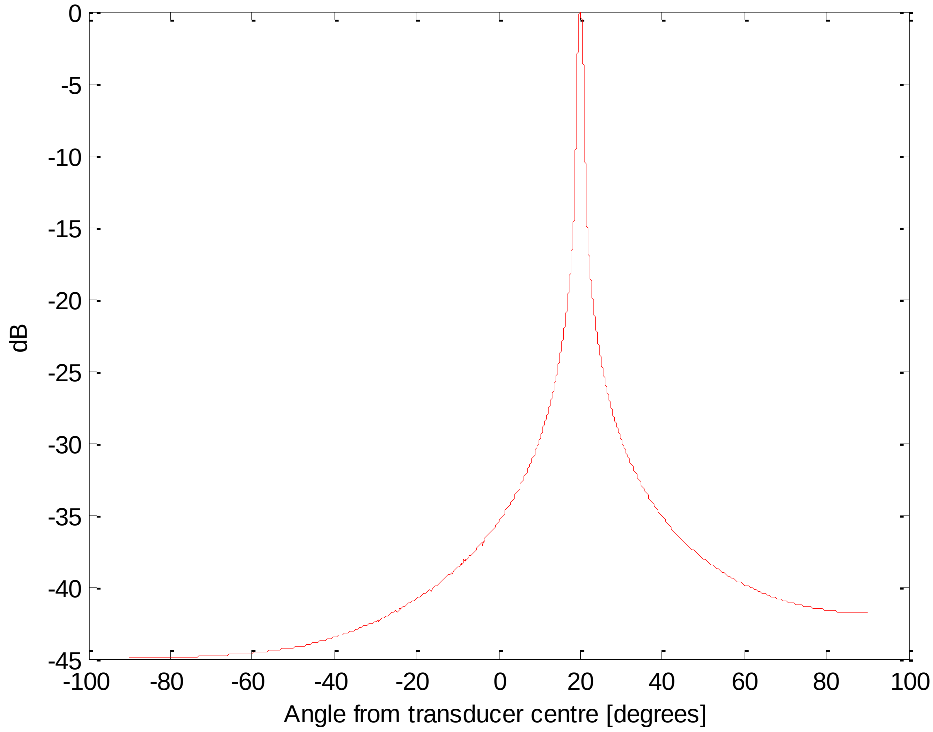

Figure 13. Beam profile of the intact transducer, steered to twenty degrees.

The increase in noise floor elevated with the number of dead elements, with the exception of fifteen grouped dead elements. For the randomised patterns of dead elements, the increase in noise-floor level was higher than for the grouped cases, see Table 5. The standard deviations were generally higher for the grouped dead elements. The noise floor increase was smaller for the edge configuration compared with the other two.

Table 5. Increase of noise floor compared to the intact transducer, which has a noise floor level of -41.8 dB.

Number of dead elements	Random [ΔdB]	Grouped [ΔdB]	Edge [ΔdB]
5	4.78 ± 2.50	3.20 ± 4.16	0.38 ± 0.08
10	5.48 ± 2.22	4.17 ± 4.00	0.80 ± 0.16
15	6.39 ± 6.76	3.97 ± 4.00	-
20	7.37 ± 1.58	4.79 ± 4.50	-
30	9.25 ± 1.42	6.45 ± 3.48	-

The average side-lobe level increased when the number of dead elements got higher and the side-lobe level was higher for grouped dead elements, see Table 6.

Table 6. Average side-lobe level when beam is steered to twenty degrees.

Number of dead elements	Random [dB]	Grouped [dB]
5	-31.7 ± 5.12	-21.9 ± 15.6
10	-28.7 ± 6.38	-18.9 ± 9.26
15	-26,4 ± 6.76	-15.0 ± 5.20
20	-23.2 ± 6.64	-15.9 ± 7.46
30	-23.2 ± 5.04	-12.65 ± 6.28

4.1.3. Forty degree steering

The beam profile of the intact transducer steered to forty degrees is presented in Figure 14, a side lobe can be visualised on the left side in the beam profile.

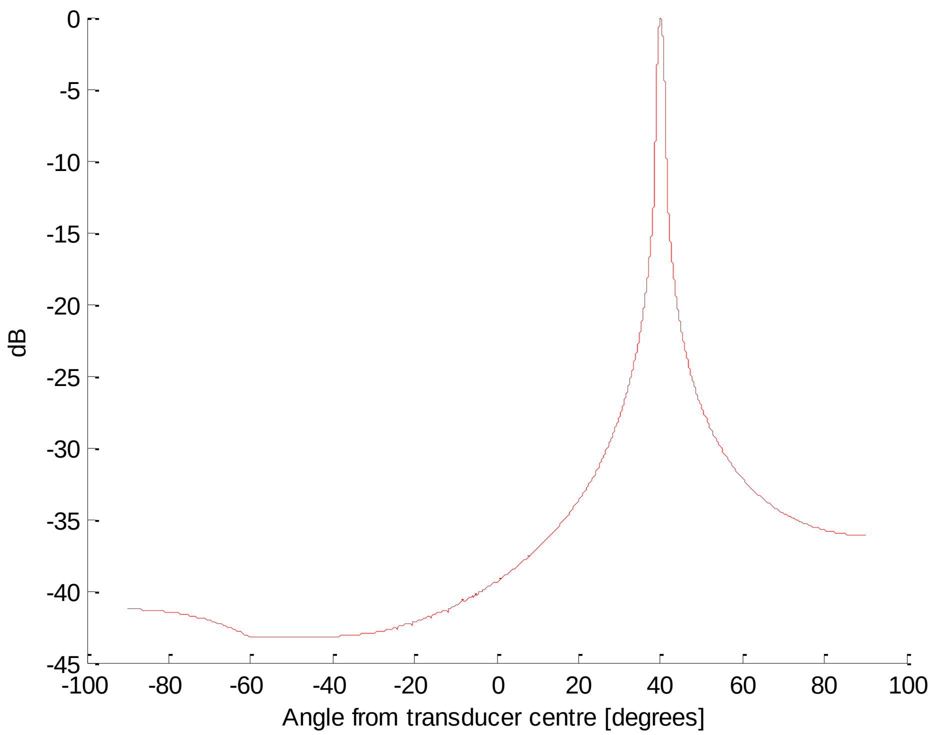

Figure 14. Beam profile of the intact transducer steered to forty degrees.

The noise floor increased with the number of dead elements, see Table 7. The noise-floor level was higher for the steered intact transducer than the non-steered. Consequently, the noise-floor levels for the broken transducers were higher for the steered cases than the non-steered case.

Table 7. Increase of noise floor compared to the intact transducer, which has a noise floor level of -36.1 dB

Number of dead elements	Random [ΔdB]	Grouped [ΔdB]	Edge [ΔdB]
5	1.40 ± 2.50	3.10 ± 2.04	0.35 ± 0.12
10	3.32 ± 4.02	4.18 ± 4.44	0.75 ± 0.24
15	4.44 ± 2.40	3.66 ± 2.83	-
20	5.35 ± 2.44	5.08 ± 4.50	-
30	6.14 ± 2.58	5.68 ± 3.14	-

The side-lobe level increased with increasing number of dead elements and the grouped formations had higher average side-lobe level than random configuration, see Table 8. As in the non-steered case, there were no side lobes present in the edge configurations.

Table 8. The average side-lobe level when the beam is steered to forty degrees.

Number of dead elements	Random [dB]	Grouped [dB]
5	-29.5 ± 10.4	-22.0 ± 13.7
10	-28.2 ± 5.36	-18.6 ± 8.84
15	-25.2 ± 6.66	-14.7 ± 4.74
20	-20.8 ± 8.64	-15.9 ± 7.46
30	-20.6 ± 9.32	-13.6 ± 9.92

4.2. Test II

The maximum intensity in the point spreader for the defect transducers compared with that of the intact is presented in Table 9. The number of dead elements affected the loss of intensity but the location of the dead elements had no visible impact. The loss of intensity was smaller for the edge configuration.

Table 9. The remaining intensity in the main lobe for the real-data simulations

Number of dead elements	Random [%]	Grouped [%]	Edge [%]
5	94.8 ± 0	94.8 ± 0	95.4 ± 0
10	89.5 ± 0	89.2 ± 0.02	90.8 ± 0
15	84.2 ± 0	84.1 ± 0.02	-
20	79.1 ± 0	78.9 ± 0.02	-
30	68.6 ± 0.02	68.5 ± 0.02	-

The SNR varied but there was no observable tendency related to the number of dead elements, see Table 10. The standard deviations were higher for the grouped configuration and it also increased with the number of dead elements.

Table 10. Signal to noise ratio for the real-data simulations.

Number of dead elements	Random [dB]	Grouped [dB]	Edge [dB]
5	35.7 ± 1.58	35.0 ± 3.06	36.2 ± 0.85
10	35.6 ± 1.80	35.1 ± 6.46	36.7 ± 1.54
15	35.8 ± 2.44	33.0 ± 7.56	-
20	35.4 ± 4.12	32.2 ± 8.81	-
30	34.8 ± 5.2	29.0 ± 8.48	-

The average width of the point spreader in -6 dB was not affected by the number of dead elements for the random and grouped configurations. The average width for the random and grouped configurations was 1.65 mm, compared to the intact transducer which had a width of 1.64 mm. The width for the edge configuration was wider and had lower standard deviations.

The intensity level in the cyst coincided with the remaining intensity in the point spreader, thus the intensity decreased with increasing number of dead elements.

4.3. Comparison of results

All comparisons in this section were made between Test I with zero degree steering and Test II.

The remaining percentage intensity in Test I corresponded to the result of Test II. The intensity loss was linear, as shown in Figure 15, the blue line shows the intensity drop according to the results in Test I and the red line shows the plot according to Equation 6.

$$Remaining\ intensity\ [\%] = \frac{Number\ of\ working\ elements}{Total\ number\ of\ elements} \cdot 100$$

Equation 6

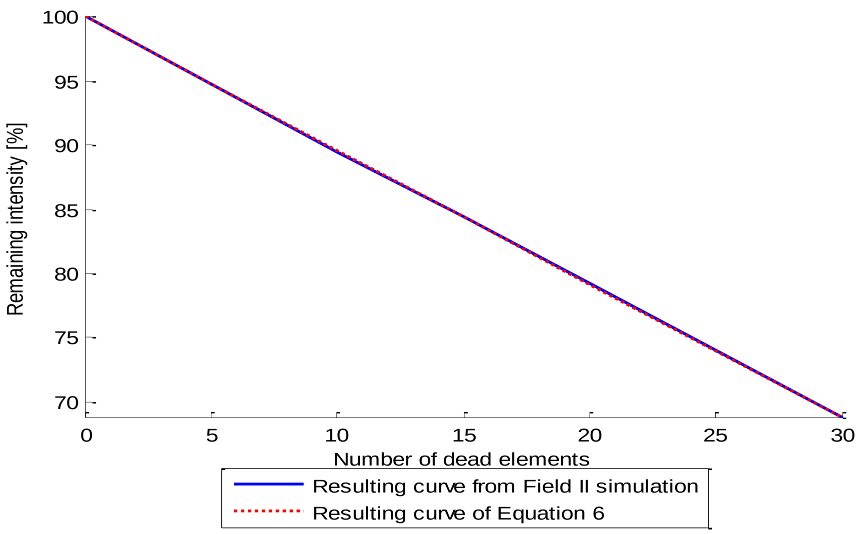

Figure 15. The intensity drop in the Field II simulation, zero degrees, and resulting curve of Equation 6

The attenuation of ultrasound, measured in decibel, is linearly proportional to the distance travelled. The intact transducer has lost half of its energy after a travelled distance of 4 cm. The defect transducers have lower original energy, and thus reach that energy level earlier. These depths are presented in Table 11 and the values are valid for the set-up in Test I.

Table 11. The distance travelled to the point where the transmitted beam of the intact transducer has lost half of its intensity.

Number of dead elements	Distance travelled [cm]
0	4.00
5	3.69
10	3.36
15	3.01
20	2.65
30	1.83

The noise-floor level in Test I was not comparable with the SNR of the point spreader in Test II, as the noise-floor level increased with the number of dead elements while no similar tendency could be observed in the SNR.

The beam width varied for different error patterns but the average beam width was unaffected by increasing number of dead elements in both tests for the random and the grouped configurations. The measurements were of the same magnitude. The patterns that yielded the widest beam width in Test I also yielded the widest measurement of the point spreader in Test II. Similarly, the error pattern causing the narrowest width in Test I corresponded to the error pattern that yielded the narrowest width in Test II. For the edge configuration, the beam widened when the number of dead elements increased from five to ten.

The intensity in the cyst decreased with increasing number of dead elements while the side-lobe level increased with the number of dead elements.

5. Discussion

Dead elements in transducers affect the beam profile. Different error configurations yield different beam profiles and the beam profile is, thus, affected by the number of dead elements and their location. Measurements from Test II imply that dead elements in transducers affect the image quality. Within the scope of this study, it cannot be established whether the two simulation types yield comparable results and hence not how the altered beam profile affects the image quality. The beam width and the loss of intensity are parameters that correspond in the tests, but there is need to further investigate other parameters to determine if there is a total correlation. An acceptance level regarding the number of dead elements cannot be determined since the location of the dead elements impacts the results.

5.1. Findings

Below follows a discussion regarding the results of this study.

5.1.1. Comparison of simulation types

The remaining intensity in the main peak coincided in the two tests. The loss of energy was, in these tests, affected only by the number of dead elements. It was not considered to be any difference in intensity loss associated with the placements of the dead elements. The width of the beam in Test II agreed with the results from Test I suggesting that this parameter can be compared for the two simulation types.

Alterations in side-lobe level were thought to yield differences in cyst intensity but no such link was found. The percentage loss of intensity in the cyst corresponded to the percentage loss of intensity in the point spreader. This indicates that there was an overall loss of intensity. If there would have been an increase of side-lobe level, the intensity in the cyst would not follow that of the point spreader. Due to the collection procedure of real data to Test II, in which all elements were active during pulse transmission, the presence of side lobes can be questioned. For side lobes to be detectable in the cyst, they must reach the location of the cyst.

There was no visible connection between the SNR for Test II and the noise-floor level for Test I. The noise floor and the SNR both affect the contrast resolution but in this study they did not coincide.

It is difficult to determine whether it is possible to compare the results of Test I with the results of Test II. The parameters that did not coincide measure the same feature, but do it differently. Therefore further studies are needed to determine whether the two simulation types are comparable and which parameters are suitable.

The results of this study show that the beam profiles in Test I, as well as the parameters of image quality from Test II, are affected by dead elements in the transducer. As the collection of data to Test II was done with all elements active during transmission, the results are not fully compatible with images obtained from an actual examination. The results are, however, considered to give indications regarding the effect on image quality due to dead elements. The overall intensity decreased with increasing number of dead elements, indicating impaired ability to image at larger depths. Some error patterns yielded alterations of the -6 dB width of point spreader and the SNR, which suggest degradation in resolution.

5.1.2. Acceptance level regarding dead elements

The collection of data for Test II was limited to one focus angle and for this reason consideration has only been given to Test I for recommendations regarding the acceptance level.

The loss of intensity in the main peak was affected by the number of dead elements compared to the number of working elements. The intensity loss is linear, suggesting that all elements contribute equally to the total beam. A beam of lower intensity will reach the point where the intact transducer has lost half of its energy at a shallower depth, resulting in decreased penetration depth. Consequently, the ability of imaging at greater depths will be reduced.

There are standard deviations of a size that indicates that the placement of the dead elements affect the beam width, however, the deviations are so small that they are not considered to be visible in an ultrasound image. The group configuration yielded higher standard deviations than the random configuration, indicating that the configuration affects the result.

The results suggest that the side-lobe level increases with the number of dead elements and that it is higher for the group configuration. Grouped elements give rise to wider gaps between functioning elements, which can result in a changed interference pattern. This could be an explanation to the increased side-lobe level for grouped dead elements. However, the standard deviations were high and not all error patterns caused side lobes, implicating that the location of the dead elements impacts the outcome of the side-lobe level.

For the edge configuration, the beam profile of the defect transducer followed that of the intact closely. This suggests that a transducer with broken elements at the edges act like a transducer with fewer elements. A test with a transducer consisting of fewer elements was constructed in Field II. The resulting beam plot was compared with the beam plot of a transducer with broken edge elements and the curves agreed, which supported the statement.

Due to the size of the standard deviations in this study, it is not possible to determine an acceptance level regarding the number of dead elements in a transducer. Consideration must be given to a larger number of parameters and it must be evaluated how they affect each other and what values are acceptable for each parameter.

The results in this study show that a transducer with five dead elements can yield the same result for certain parameters as one with thirty dead elements. This indicates that the placement, as well as the number, of dead elements has an impact on the beam profile. Consequently, there is need for further studies regarding the effect of different error patterns.

5.2. Methodological issues

As previously mentioned only a selected number of error patterns have been considered. The placement of each dead element have been randomised, instead of selected, to obtain a more even distribution. In reality, dead elements occur due to a number of reasons, which are prone to yield different error patterns.

The simulated transducers consisted of 96 elements while the real transducer consists of 192 elements. This set-up was selected to simplify the simulation and the disablement of elements. In real images, the outer rows help focus the beam to enable thinner slice thickness, which is a parameter that is not evaluated in this study.

The collected images used in the Test II were obtained by transmitting ultrasound from all elements. Side lobes due to dead elements might therefore not have arisen and consequently the results are not fully comparable to real images collected with faulty transducers.

Measurements in Test I were taken at a depth of 7.76 cm, which was also the focus depth of the transducer in the simulations. In Test II, the point spreader evaluated was located at a depth of 7.76 cm. The focus of the transducer was, however, at a depth of 8.08 cm. The receive focus of the M5S-D transducer is dynamic and can change between different examinations. It was decided to make the measures at the focus depth in Test I as it yields the most accurate values of the transducer function.

Steering to twenty and forty degrees in Test I has been done only to the right. As a result, the indices of the dead elements affect the outcome. In a more extensive study it would have been interesting to steer the beam in both directions for all error patterns.

There is no clear definition of side lobes and it is, therefore, difficult to determine what constitutes side lobes in beam profiles. No consideration has been given to the width of the side lobes, their position in the lateral direction or other lobes than the highest one on each side of the main lobe. Additionally, the mean value of an error-pattern set is taken for those error patterns yielding side lobes.

According to Equation 4, at page 8, the rendered ultrasound image is the result of the convolution of the actual object and the impulse response of the equipment. In Field II the actual object has a very small extension and is described by a Dirac-function, while the object in the Test II has a small extension. The beam widths of the two experiments are, therefore, not fully corresponding. The impact is, however, considered to be small and is therefore disregarded.

The edge configuration did not yield different beam profiles for different error patterns with five or ten dead elements. Therefore, it was assumed that the beam profiles from transducers with a larger number of dead elements would not diverse from this pattern.

The evaluation done was objective, that is, measured values were compared to obtain results regarding image quality. It is however problematic that these parameters do not always coincide to a viewer's perception of the image [4, 13]. This especially applies to the MSE-parameter [17] and hence, it was not considered in this study. Furthermore, axial resolution is directly related to the pulse length which is, as described in section 2.3, affected by the frequency and number of pulse cycles. Therefore, the axial resolution is not affected by dead elements and not evaluated in this study. Slice thickness, low-contrast penetration depth and dynamic range are examples of parameters that were not included as they were not possible to measure within the scope of this study.

There are many parameters that describe contrast resolution. In this study, the parameters chosen were SNR, average side-lobe level and noise-floor level. This choice was made as these parameters were measurable and that they were thought to be comparable.

6. Conclusion

The simulations in Field II show that different error patterns affect the beam profile. The intensity loss, in the main peak, is only affected by the number of dead elements. The location of the dead elements and the beam steering does not affect the outcome. Furthermore, the noise floor increases with the number of dead elements and with beam steering. The high standard deviation suggests that the location of the dead elements impacts the noise-floor level.

From the chosen method of the side-lobe measurement in this study, it can be concluded that the average side-lobe level increases with increasing numbers of dead elements. Grouped dead elements generate higher side lobes than randomly spread dead elements and thus the placement and configuration affect the average side-lobe level.

Dead elements only at the edges of the transducer surface yields beam profile slightly wider and with a slightly increased noise floor compared with the beam profile of an intact transducer.

It has been determined that the beam profiles are altered by dead elements in transducers and that the placement of the dead elements affects the outcome. It has not been determined how an altered beam profile affects the image quality, but it is likely that dead elements lead to degradation of image quality.

In this study, it cannot be determined if a simulation using Field II is comparable with a real-data simulation. Some parameters evaluated coincide but there is a need for further studies to find the most suitable parameters in order to determine whether the two simulation types are comparable.

As both the number of dead elements and their placement affect the beam profile, an acceptance level could not be suggested regarding the number of dead elements.

References

[1] M. Mårtensson, "Evaluation of Errors and Limitations in Ultrasound Imaging Systems," Ph.D. dissertation, School of Technology and Health, Royal Institute of Technology, Stockholm, 2011.

[2] J. A. Jensen and N. B. Svendsen, "Calculations of pressure fields from arbitrarily shaped, apodized, and excited ultrasound transducers," *IEEE Trans. Ultrason. Ferroelectr. Freq. Control*, vol. 39, pp. 262-267, Mar. 1992.

[3] B. Weigang *et al.*, "The Methods and Effects of Transducer Degradation on Image Quality and the Clinical Efficacy of Diagnostic Sonography," *Journal of Diagnostic Medical Sonography,* vol. 19, pp. 4-13, Jan. 2003.

[4] P. Hoskins *et al.*, *Diagnostic Ultrasound -Physics and Equipment*, 2nd ed. Cambridge, United Kingdom: Cambridge University Press, 2010.

[5] P. Allisy-Roberts and J. Williams, *Farr's Physics for Medical Imaging*, 2nd ed. Philadelphia: WB Saunders Company, 2008.

[6] J. T. Bushberg *et al.*, *The Essential Physics of Medical Imaging*, 3rd ed. Philadelphia: Lippincott Williams & Wilkins, 2012.

[7] S. Holm and K. Kristoffersen, "Analysis of Worst-Case Phase Quantization Sidelobes in Focused Beamforming," *IEEE Trans. Ultrason. Ferroelectr. Freq. Control,* vol. 39, pp. 593-599, Mar. 1992.

[8] B. A. J. Angelsen, "Ultrasound Imaging - Waves, Signals, and Signal Processing," vol. 1, 1st ed. Trondheim, Norway: Emantec AS, 2000.

[9] L. Smith *et al.*, "Enhancing Image Quality Using Advanced Signal Processing Techniques," *Journal of Diagnostic Medical Sonography,* vol. 24, pp. 72-81, Mar. 2008.

[10] T. L. Szabo, *Diagnostic ultrasound imaging: inside out*, 1st ed. Burlington: Elsevier Academic Press, 2004.

[11] B. A. J. Angelsen, "Ultrasound Imaging - Waves, Signals, and Signal Processing," vol. 2, 1st ed. Trondheim, Norway: Emantec AS, 2000.

[12] A. Vretblad, *Fourier Analysis and Its Applications*, 1st ed. New York: Springer-Verlag, 2003.

[13] K. S. Rangaraju *et al.*, "Review Paper on Quantitative image quality assessment - Medical Ultrasound Images," *International Journal of Engineering Research & Technology,* vol. 1, pp. 1-6, Jun. 2012.

[14] M. Chambah *et al.*, "Towards an Automatic Subjective Image Quality Assessment System," Proc. of SPIE, vol 7242, 2009.

[15] J. A. Jensen, "A program for simulating ultrasound systems," *Med. Biol. Eng. Comp.,* vol. 4, pp. 351-353, 1996.

[16] *User's guide for the Field II program*, 3.2 ed, J. A. Jensen, 2010, Available: http://field-ii.dk/?users_guide.html.

[17] Z. Wang and A. C. Bovik, "A Universal Image Quality Index," *IEEE Signal Process. Lett.*, vol. 9, pp. 81-84, Mar. 2002.

Appendix

Appendix 1

The code that was used to do the Field II simulations is presented below.

```
% Field simulation of one intact transducer and 'no_broken' with an error
% pattern decided by 'enabled'. The pressure field of each transducer are
% calculated in dB as a function of angle from the transducer centre.
clc
clf
close ALL
clear ALL;
field_init
```

Variabels

```
%The beam
f0 = 3e6 ;                          %Centre frequency
fs = 100e6 ;                        %Sampling frequency
c = 1540 ;                          %Velocity of tissue
lambda = c/f0  ;                    %Wave length when f=f0
no_periods = 2;                     %Number of cycles in pulse
sector_width = pi;                  %Sector width
theta = -sector_width/2;            %The edge angle on sector's left side
angle = 0;                          %Focus angle [degrees]

% calc_theta determines the points in which pressure is measured. The
% points are more concentrated around focus.
[theta_values, index_rms] = calc_theta(angle);

% The transducer
no_element_x = 96;                  %Number of elements x-direction
height = 12/1000;                   %The height of the elements [m]
width = (20/no_element_x)/1000;     %Width of elements [m]
no_element_y = length(height);      %Number of elements y-direction
kerf_x = width/10;                  %Distance between two elements(x-dir)
kerf_y = width/10;                  %Distance between two elements(y-dir)
sub_x = 1;                          %Mathematical objects x-dir.
sub_y = 9;                          %Mathematical objects y-dir.
focus = [0 0 77.6]/1000;            %Electronic focus of transducer (xyz)

% Other parameters
Z = 1.480e6;                        %Acoustic impedance [kg/(m^2*s)]
r = 77.6/1000;                      %Radial distance [m]
angle = angle*pi/180;               %Angle in rad.
excitation = sin(2*pi*f0*...
    (0:1/fs:1.5/f0));               %Definition of excitation
```

```
impulse = gauspuls(-2/f0...
    :1/fs:2/f0,f0,1.0);
% Sampling frequency for the entire system
set_sampling(fs);
set_field('freq_att', 0.5*100/(1e6) );
set_field('att_f0', f0) ;

% Code that decides which elements are dead.
no_broken = 5;
enabled_all = enabled_five;       %Function to collect 10 sets of 5...
                                     ...dead elements

% Create matrices for storage of data
no_tests = 10;                    %Number of broken transducers
results = zeros(no_tests+1, 3);
broken_elem = zeros(no_tests, no_broken);
dB=[];
```

Simulation of intact transducer

```
% Create intact transducer
enabled_hel = ones(no_element_x, no_element_y);
Th_intact = xdc_2d_array(no_element_x, no_element_y, width, height, ...
        kerf_x, kerf_y, enabled_hel, sub_x, sub_y, focus );

% Define the excitation pulse and impulse response for intact transducer.
xdc_excitation(Th_intact, excitation);
xdc_impulse(Th_intact, impulse);
xdc_focus(Th_intact, 0, [r*sin(angle) 0 r*cos(angle)]); % Beam steering

% Calculate the pressure field (hp) in the points given by 'points'
points = [sin(theta_values)' zeros(size(theta_values))'...
    cos(theta_values)']*r;
[hp_intact,t_intact]  =calc_hp(Th_intact, points);

P_intact = max(abs(hilbert(hp_intact)));

dB(1,:) = 20*log10(P_intact/max(P_intact));

%Calculate the beam width in -3 dB and -6 dB, using calc_dist.
[angle_diff, ~] = calc_dist2(dB(1,:), 3, theta_values);
dist_radial = (angle_diff*r)*1000 ;
results(1,1) = dist_radial ;

[angle_diff, ~] = calc_dist2(dB(1,:), 6, theta_values);
dist_radial = (angle_diff*r)*1000 ;
results(1,2) = dist_radial ;
```

Simulation of broken transducers

```
for k = 2:(1+no_tests) %'no_tests' different error patterns are run

    % Create broken transducer with errors according to enable_broken
    enabled = enabled_all(k-1, :)' ; %Error pattern for this k
    noll = enabled';

    % Store the indices of dead elements
    if no_broken == 0
        disp('No broken elements');
    else
        % Indices of dead elements are stored
        vect_zeros = find(noll == min(noll));
        broken_elem(k-1, :) = vect_zeros;
    end

    % Create the transducer with broken elements
    Th = xdc_2d_array(no_element_x, no_element_y, width, height, ...
            kerf_x, kerf_y, enabled, sub_x, sub_y, focus );

    % Define the excitation pulse and impulse response.
    xdc_excitation(Th, excitation);
    xdc_impulse(Th, impulse);
    xdc_focus(Th, 0, [r*sin(angle) 0 r*cos(angle)]);

    % Calculate the pressure field, hp, in 'points'
    [hp_broken,t_broken] = calc_hp(Th, points);

    P_broken = max(abs(hilbert(hp_broken)));
    dB_ref = 20*log10(P_broken/max(P_intact));
    dB(k,:) = 20*log10(P_broken/max(P_broken)); % Broken transducer,
                                                 ...normalized to 0 dB

    % Calculate the beam width in -3 dB and -6 dB using the
    % function calc_dist
    [angle_diff, ~] = calc_dist2(dB(k,:), 3, theta_values);
    dist_radial = (angle_diff*r)*1000 ;
    results(k,1) = dist_radial ;

    [angle_diff, ~] = calc_dist2(dB(k,:), 6, theta_values);
    dist_radial = (angle_diff*r)*1000 ;
    results(k,2) = dist_radial ;

% Calculate the the lowering of intensity in the main peak
    results(k,3) = max(dB(1,:))-max(dB_ref);


    %Plot the dB_curve for intact and broken transducer in the same graph
```

```
    figure
    hold on
    plot(theta_values*180/pi, dB(k,:)),'-b';  % Broken no. k
    plot(theta_values*180/pi, dB(1,:), '-r'); % Intact
    hold off
    title ('dB-plot at a radius of 7.76 cm from transducer')
    xlabel('Angle from transducer centre [degrees]')
    ylabel('dB')
    legend('Transducer with broken elements','Intact transducer',...
        'Location','southoutside' )
end

%Plot all dB curves in one graph
figure
plot(theta_values*180/pi, dB);
legend('Intact','1','2','3','4','5','6','7','8','9','10');

% Write results to Excel
xlswrite('Five_random.xlsx', results, 'Blad1', 'B2');
xlswrite('Five_random.xlsx', broken_elem, 'Blad2', 'B2');
save ('dB_five.mat', 'dB') % Store dB matrix

%Release transducer and end Field
xdc_free(Th);
field_end;
```

Appendix 2

In this section the indices of the dead elements in each test are presented.

Five random elements

Pattern no.	Indices of dead elements				
1	16	47	77	92	94
2	14	41	77	88	93
3	4	63	66	82	90
4	17	38	63	72	73
5	4	5	10	27	68
6	4	31	67	80	92
7	18	37	43	74	77
8	43	48	63	69	73
9	12	16	27	63	66
10	22	33	48	57	93

Five grouped elements

Pattern no.	Indices of dead elements				
1	43	44	45	46	47
2	37	74	75	76	77
3	18	19	48	77	78
4	25	26	27	28	29
5	63	64	65	66	67
6	27	28	69	70	71
7	63	66	67	68	69
8	12	16	17	18	19
9	48	49	50	51	93
10	22	33	34	57	73

Five edge elements

Pattern no.	Indices of dead elements				
1	1	2	3	4	5
2	1	2	3	4	5
3	1	93	94	95	96
4	1	2	3	4	5
5	1	2	3	4	96
6	1	93	94	95	96
7	1	2	94	95	96
8	1	2	3	95	96
9	1	2	3	4	5
10	1	93	94	95	96

Ten random elements

Pattern no.	Indices of dead elements									
1	10	13	27	53	61	79	87	88	92	93
2	14	16	41	47	63	77	88	92	93	94
3	4	17	38	63	66	68	72	73	82	90
4	4	5	10	27	31	37	43	67	80	92
5	18	27	43	48	63	66	69	73	74	77
6	12	16	22	25	33	48	57	63	73	93
7	14	15	25	49	53	68	79	81	86	93
8	19	24	25	34	46	53	57	60	80	90
9	6	8	28	37	51	55	73	75	89	90
10	2	13	16	30	33	46	51	55	58	77

Ten grouped elements

Pattern no.	Indices of dead elements									
1	8	9	10	43	52	53	54	55	56	57
2	1	2	3	4	5	11	12	93	94	95
3	75	76	77	78	79	80	81	82	83	84
4	9	10	11	12	39	79	80	84	85	86
5	25	26	27	28	29	30	31	32	33	34
6	42	43	77	78	79	80	81	82	83	84
7	14	15	16	18	26	27	28	29	30	88
8	14	56	60	61	62	63	84	85	86	87
9	34	35	36	39	40	50	51	52	53	54
10	8	9	10	24	25	26	27	28	29	30

Ten edge elements

Pattern no.	Indices of dead elements									
1	1	2	3	4	5	6	7	8	9	10
2	1	2	3	4	5	92	93	94	95	96
3	1	2	3	4	5	6	7	8	9	96
4	1	2	89	90	91	92	93	94	95	96
5	1	2	3	4	5	92	93	94	95	96
6	1	2	3	4	5	6	7	8	9	10
7	1	2	3	4	5	6	7	8	95	96
8	87	88	89	90	91	92	93	94	95	96
9	1	2	3	4	5	6	7	94	95	96
10	1	88	89	90	91	92	93	94	95	96

Fifteen random elements

Pattern no.	Indices of dead elements														
1	10	13	14	16	27	47	53	61	77	79	87	88	92	93	94
2	4	17	27	38	41	63	66	68	72	73	77	82	88	90	93
3	4	5	10	18	31	37	43	48	63	67	69	74	77	80	92
4	12	16	22	25	27	33	48	49	57	63	66	68	73	86	93
5	14	15	19	24	25	34	46	53	57	60	79	80	81	90	93
6	2	6	8	13	28	33	37	46	51	53	55	73	75	89	90
7	9	15	16	22	26	30	44	51	58	63	67	72	77	80	88
8	1	8	9	11	25	39	42	43	52	75	77	79	84	93	96
9	8	12	14	18	24	26	34	39	50	53	56	60	82	84	88
10	5	10	11	18	24	33	36	38	39	41	47	48	75	87	91

Fifteen grouped elements

Pattern no.	Indices of dead elements														
1	15	16	17	18	19	20	21	22	23	24	25	26	27	81	82
2	19	20	25	26	27	28	29	30	31	32	33	34	79	90	91
3	25	26	27	28	29	30	31	32	33	34	35	36	37	38	39
4	34	46	60	61	62	63	64	65	66	67	68	69	70	71	72
5	53	54	55	56	57	80	81	82	83	84	85	86	87	88	89
6	28	29	44	45	46	47	48	49	50	51	52	53	54	55	73
7	8	37	38	39	40	41	55	75	76	77	78	79	80	81	90
8	13	14	15	16	17	18	19	20	21	22	23	24	55	56	57
9	2	3	4	5	6	7	33	34	46	47	48	49	50	51	52
10	16	17	18	19	20	21	22	23	24	25	30	51	52	58	77

APPENDIX

Twenty random elements

Pattern no.	Indices of dead elements									
1	4	10	13	14	16	27	41	47	53	61
	63	77	79	82	87	88	90	92	93	94
2	4	5	10	17	18	27	31	37	38	43
	63	66	67	68	72	73	74	77	80	92
3	12	14	15	16	22	25	27	33	43	48
	49	53	57	63	66	68	69	73	86	93
4	6	8	19	24	25	28	34	37	46	51
	53	55	57	60	73	79	80	81	89	90
5	2	9	13	16	22	26	30	33	44	46
	51	55	58	63	67	72	75	77	88	90
6	1	8	9	11	15	18	25	26	39	42
	43	52	75	77	79	80	84	88	93	96
7	5	8	12	14	18	24	33	34	39	41
	47	48	50	53	56	60	82	84	87	91
8	2	5	6	10	11	13	17	23	24	34
	36	38	39	56	63	75	79	87	91	92
9	8	18	19	29	30	36	42	43	44	47
	49	50	53	61	63	66	71	72	75	90
10	17	19	20	22	23	29	34	37	46	52
	53	57	60	62	77	78	79	82	85	91

Twenty grouped elements

Pattern no.	Indices of dead elements									
1	3	4	5	6	7	18	19	20	21	22
	24	25	26	27	28	29	30	86	87	88
2	6	7	17	18	48	49	50	51	52	53
	54	55	56	66	69	70	71	94	95	96
3	5	6	7	8	9	10	11	12	13	15
	16	51	52	53	54	55	56	70	71	79
4	50	51	52	53	54	55	56	64	65	66
	67	68	77	78	79	80	81	82	83	84
5	9	10	11	44	45	46	47	48	49	50
	51	52	53	80	81	82	83	84	85	86
6	13	17	18	19	20	21	22	23	24	25
	26	27	28	29	30	31	32	33	38	39
7	6	7	8	9	10	11	12	13	14	39
	51	52	53	80	81	82	83	84	85	86
8	41	42	43	44	45	46	47	48	49	50
	51	52	53	54	55	64	65	66	67	68
9	2	3	4	29	30	42	61	62	63	64
	65	66	67	68	69	70	71	72	73	74
10	17	18	19	20	21	22	23	24	25	26
	27	28	29	36	37	38	39	40	41	42

Thirty random elements

Pattern no.	Indices of dead elements														
1	4	5	10	13	14	16	17	27	31	38	41	47	53	61	63
	66	67	68	72	73	77	79	80	82	87	88	90	92	93	94
2	4	12	14	15	16	18	22	24	25	27	33	37	43	48	49
	53	57	63	66	68	69	73	74	77	79	81	86	90	92	93
3	2	6	8	13	16	19	25	26	28	30	33	34	37	44	46
	51	53	55	57	58	60	63	67	72	73	75	77	80	89	90
4	1	8	9	11	12	14	15	18	22	24	25	26	34	39	42
	43	50	52	53	56	60	75	77	79	80	82	84	88	93	96
5	2	5	6	10	11	13	17	18	23	24	29	33	34	36	38
	39	41	44	47	48	53	56	63	71	72	75	79	87	91	92
6	8	18	19	20	23	29	30	34	36	37	42	43	46	47	49
	50	52	53	57	60	61	62	66	75	77	78	79	85	90	91
7	3	9	11	12	17	18	19	22	23	25	26	29	30	31	40
	41	42	43	47	49	56	58	69	71	77	82	87	89	90	95
8	3	4	10	11	14	19	23	26	33	36	38	45	47	48	51
	53	60	63	66	68	69	70	75	77	85	86	87	88	93	95
9	3	5	6	7	10	15	17	18	24	46	47	48	49	50	51
	56	59	60	63	64	66	69	70	72	78	79	83	86	87	94
10	2	6	9	11	13	17	20	26	29	33	36	38	39	41	42
	44	48	51	53	61	64	68	71	77	78	80	89	91	92	95

Thirty grouped elements

Pattern no.	Indices of dead elements														
1	1	34	35	36	37	38	39	40	41	42	43	44	45	46	47
	48	49	50	51	52	53	65	66	67	75	76	77	78	79	80
2	1	38	39	40	41	42	43	44	45	46	47	48	49	50	51
	52	53	54	58	79	80	81	82	83	84	85	86	87	88	89
3	4	31	32	45	46	47	48	49	74	75	76	77	78	79	80
	81	82	83	84	85	86	87	88	89	90	91	92	93	94	95
4	17	18	19	20	21	22	23	24	25	26	27	28	29	30	31
	32	33	34	35	46	47	48	49	59	60	61	70	71	72	89
5	9	10	11	12	13	14	15	16	17	18	26	27	28	29	30
	31	32	33	34	35	36	37	38	39	40	41	42	43	74	75
6	12	21	22	23	41	44	45	56	57	58	59	60	61	62	63
	64	65	66	67	68	69	70	71	72	73	91	92	93	94	95
7	25	26	34	35	36	37	38	39	40	41	42	43	64	65	66
	67	68	69	70	71	72	73	74	75	76	77	78	79	81	82
8	12	13	14	15	16	17	18	19	26	27	28	29	30	31	32
	33	34	35	36	37	38	39	40	41	47	59	60	61	62	91
9	11	21	22	23	24	25	26	27	28	29	30	31	32	33	34
	35	62	63	64	65	66	67	68	69	70	71	72	73	74	75
10	11	12	13	14	15	16	17	18	39	40	41	42	43	44	45
	46	47	48	49	50	51	52	53	61	62	63	74	75	76	90

Appendix 3

In this section, tables of the results from Test I, with the beam steered to zero degrees, are presented. The measurements are taken at a depth of 7.76 cm. The noise floor level for the intact transducer is -45.6 dB and the values presented under “Noise floor increase” are the deviations from this.

Five random elements

Pattern no.	-3 dB beam width [mm]	-6 dB beam width [mm]	Remaining intensity [%]	Average side lobe level [dB]	Noise floor increase [ΔdB]
Intact	1.67	2.30	-	-	-
1	1.70	2.35	94.8	-33.9	8.03
2	1.70	2.35	94.8	-33.4	5.95
3	1.70	2.34	94.8	-30.7	6.46
4	1.66	2.29	94.8	-30.5	5.81
5	1.71	2.36	94.8	-30.5	5.91
6	1.70	2.34	94.8	-32.6	5.98
7	1.66	2.29	94.8	-35.0	6.71
8	1.64	2.26	94.8	-35.1	5.73
9	1.67	2.30	94.8	-35.8	6.44
10	1.67	2.29	94.8	-33.8	5.98
Mean	1.68	2.32	94.8	-33.1	6.30
SD	0.024	0.034	0.000	1.99	0.69

Five grouped elements

Pattern no.	-3 dB beam width [mm]	-6 dB beam width [mm]	Remaining intensity [%]	Average side lobe level [dB]	Noise floor increase [ΔdB]
Intact	1.67	2.30	-	-	-
1	1.62	2.24	94.8	-14.4	0.47
2	1.67	2.30	94.8	-20.4	5.68
3	1.67	2.30	94.8	-22.8	5.60
4	1.66	2.29	94.8	-18.7	0.50
5	1.65	2.27	94.8	-	0.49
6	1.66	2.28	94.8	-19.9	2.69
7	1.65	2.27	94.8	-18.3	6.39
8	1.70	2.35	94.8	-21.4	5.80
9	1.65	2.27	94.8	-14.8	5.97
10	1.65	2.27	94.8	-29.8	5.77
Mean	1.66	2.29	94.8	-20.0	3.94
SD	0.019	0.030	0.00	4.60	2.58

Five edge elements

Pattern no.	-3 dB beam width [mm]	-6 dB beam width [mm]	Remaining intensity [%]	Average side lobe level [dB]	Noise floor increase [ΔdB]
Intact	1.67	2.30	-	-	-
1	1.76	2.43	94.8	-	0.60
2	1.76	2.43	94.8	-	0.60
3	1.76	2.43	94.8	-	0.54
4	1.76	2.43	94.8	-	0.60
5	1.76	2.43	94.8	-	0.54
6	1.76	2.43	94.8	-	0.54
7	1.76	2.43	94.8	-	0.48
8	1.76	2.43	94.8	-	0.48
9	1.76	2.43	94.8	-	0.60
10	1.76	2.43	94.8	-	0.54
Mean	1.76	2.43	94.8	-	0.55
SD	0.00	0.00	0.00	-	0.05

Ten random elements

Pattern no.	-3 dB beam width [mm]	-6 dB beam width [mm]	Remaining intensity [%]	Average side lobe level [dB]	Noise floor increase [ΔdB]
Intact	1.67	2.30	-	-	-
1	1.72	2.39	89.6	-25.7	7.50
2	1.72	2.37	89.6	-23.9	8.14
3	1.68	2.33	89.6	-19.9	7.90
4	1.70	2.35	89.6	-30.0	6.45
5	1.63	2.26	89.6	-19.3	7.48
6	1.67	2.29	89.6	-33.4	7.15
7	1.69	2.34	89.6	-	8.10
8	1.64	2.26	89.6	-30.0	6.88
9	1.69	2.33	89.6	-27.6	8.38
10	1.66	2.28	89.6	-25.3	8.50
Mean	1.68	2.32	89.6	-26.1	7.65
SD	0.031	0.045	0.000	4.67	0.67

Ten grouped elements

Pattern no.	-3 dB beam width [mm]	-6 dB beam width [mm]	Remaining intensity [%]	Average side lobe level [dB]	Noise floor increase [ΔdB]
Intact	1.67	2.30	-	-	-
1	1.64	2.25	89.6	-13.8	6.13
2	1.85	2.56	89.6	-28.3	5.28
3	1.72	2.42	89.6	-17.6	1.08
4	1.73	2.41	89.6	-22.4	6.15
5	1.63	2.26	89.6	-15.1	1.02
6	1.70	2.36	89.6	-18.6	2.19
7	1.69	2.35	89.6	-19.4	8.07
8	1.68	2.32	89.6	-22.5	6.32
9	1.58	2.17	89.6	-12.7	2.30
10	1.70	2.36	89.6	-19.0	1.07
Mean	1.69	2.34	89.6	-18.9	3.96
SD	0.071	0.11	0.000	4.63	2.68

Ten edge elements

Pattern no.	-3 dB beam width [mm]	-6 dB beam width [mm]	Remaining intensity [%]	Average side lobe level [dB]	Noise floor increase [ΔdB]
Intact	1.67	2.30	-	-	-
1	1.87	2.58	89.6	-	1.19
2	1.87	2.57	89.6	-	0.91
3	1.87	2.58	89.6	-	1.14
4	1.87	2.58	89.6	-	1.10
5	1.87	2.57	89.6	-	0.91
6	1.87	2.58	89.6	-	1.19
7	1.87	2.58	89.6	-	1.10
8	1.87	2.58	89.6	-	1.19
9	1.87	2.58	89.6	-	1.04
10	1.87	2.58	89.6	-	1.14
Mean	1.87	2.58	89.6	-	1.09
SD	0.00	0.003	0.00	-	0.10

Fifteen random elements

Pattern no.	-3 dB beam width [mm]	-6 dB beam width [mm]	Remaining intensity [%]	Average side lobe level [dB]	Noise floor increase [ΔdB]
Intact	1.67	2.30	-	-	-
1	1.75	2.42	84.4	-23.0	8.79
2	1.70	2.36	84.4	-30.0	8.81
3	1.69	2.33	84.4	-20.4	8.41
4	1.64	2.27	84.4	-29.9	8.67
5	1.67	2.31	84.4	-21.3	8.16
6	1.69	2.33	84.4	-27.2	8.96
7	1.66	2.28	84.4	-29.1	7.73
8	1.73	2.39	84.4	-22.4	9.04
9	1.67	2.30	84.4	-24.4	8.72
10	1.67	2.31	84.4	-28.4	8.65
Mean	1.69	2.33	84.4	-25.6	8.59
SD	0.033	0.047	0.000	3.71	0.40

Fifteen grouped elements

Pattern no.	-3 dB beam width [mm]	-6 dB beam width [mm]	Remaining intensity [%]	Average side lobe level [dB]	Noise floor increase [ΔdB]
Intact	1.67	2.30	-	-	-
1	1.72	2.41	84.4	-15.3	4.40
2	1.66	2.31	84.4	-14.6	6.83
3	1.60	2.22	84.4	-12.6	1.56
4	1.59	2.21	84.4	-13.7	6.70
5	1.74	2.42	84.4	-19.3	1.65
6	1.55	2.11	84.3	-11.1	6.76
7	1.67	2.29	84.4	-18.7	6.91
8	1.70	2.38	84.4	-16.2	1.61
9	1.69	2.32	84.3	-13.0	5.49
10	1.67	2.31	84.4	-16.0	6.83
Mean	1.66	2.30	84.4	-15.0	4.88
SD	0.061	0.098	0.000	2.62	2.39

Twenty random elements

Pattern no.	-3 dB beam width [mm]	-6 dB beam width [mm]	Remaining intensity [%]	Average side lobe level [dB]	Noise floor increase [ΔdB]
Intact	1.67	2.30	-	-	-
1	1.78	2.47	79.2	-23.8	10.1
2	1.67	2.31	79.2	-17.0	8.77
3	1.63	2.25	79.1	-30.6	9.27
4	1.65	2.27	79.2	-26.1	9.39
5	1.65	2.28	79.2	-26.4	9.55
6	1.76	2.45	79.2	-22.0	9.82
7	1.66	2.28	79.2	-24.7	9.30
8	1.75	2.43	79.2	-24.8	9.40
9	1.58	2.16	79.1	-13.9	9.13
10	1.63	2.25	79.2	-19.1	9.28
Mean	1.66	2.31	79.2	-22.9	9.40
SD	0.065	0.10	0.000	4.96	0.36

Twenty grouped elements

Pattern no.	-3 dB beam width [mm]	-6 dB beam width [mm]	Remaining intensity [%]	Average side lobe level [dB]	Noise floor increase [ΔdB]
Intact	1.67	2.30	-	-	-
1	1.83	2.58	79.2	-17.0	5.93
2	1.65	2.26	79.1	-12.7	7.88
3	1.74	2.41	79.2	-14.3	8.19
4	1.63	2.30	79.1	-18.9	2.18
5	1.64	2.26	79.1	-13.6	1.99
6	1.68	2.42	79.2	-13.4	7.39
7	1.80	2.49	79.2	-18.9	7.22
8	1.50	2.04	79.1	-9.17	2.05
9	1.63	2.26	79.2	-12.9	7.2
10	1.64	2.32	79.2	-20.9	2.17
Mean	1.67	2.33	79.2	-15.2	5.22
SD	0.095	0.15	0.00	3.60	2.75

Thirty random elements

Pattern no.	-3 dB beam width [mm]	-6 dB beam width [mm]	Remaining intensity [%]	Average side lobe level [dB]	Noise floor increase [ΔdB]
Intact	1.67	2.30	-	-	-
1	1.78	2.49	68.8	-23.2	11.3
2	1.68	2.31	68.7	-19.9	10.9
3	1.61	2.21	68.8	-25.2	10.8
4	1.73	2.40	68.8	-19.9	11.1
5	1.68	2.32	68.8	-27.7	10.6
6	1.55	2.13	68.7	-13.1	10.3
7	1.68	2.34	68.7	-20.6	10.8
8	1.69	2.34	68.7	-23.9	11.4
9	1.68	2.32	68.7	-13.8	10.5
10	1.67	2.31	68.8	-25.6	11.1
Mean	1.68	2.32	68.7	-21.3	10.9
SD	0.062	0.097	0.000	4.86	0.35

Thirty grouped elements

Pattern no.	-3 dB beam width [mm]	-6 dB beam width [mm]	Remaining intensity [%]	Average side lobe level [dB]	Noise floor increase [ΔdB]
Intact	1.67	2.30	-	-	-
1	1.47	2.01	68.7	-9.00	3.30
2	1.59	2.20	68.7	-9.54	11.5
3	2.06	2.85	68.8	-14.3	8.86
4	1.57	2.20	69.8	-12.8	8.55
5	1.70	2.50	68.7	-17.4	5.76
6	1.64	2.30	68.8	-12.1	9.10
7	1.55	2.16	68.8	-11.7	9.14
8	1.61	2.30	68.7	-18.4	8.75
9	1.54	2.12	68.7	-10.9	8.60
10	1.54	2.11	68.7	-11.1	8.69
Mean	1.63	2.27	68.8	-12.7	8.22
SD	0.16	0.24	0.003	3.12	2.20

Appendix 4

Below are the total results from Test I with twenty degree steering. The measurements are taken at a depth of 7.76 cm. The noise floor for the intact transducer is -41.2 dB and the values given for "Noise floor increase" are the deviation from that.

Five random elements

Pattern no.	-3 dB beam width [mm]	-6 dB beam width [mm]	Remaining intensity [%]	Average side lobe level [dB]	Noise floor increase [ΔdB]
Intact	1.79	2.46	-	-	-
1	1.82	2.51	94.7	-33.5	3.97
2	1.82	2.51	94.7	-33.1	3.71
3	1.81	2.50	94.8	-30.4	5.94
4	1.77	2.44	94.8	-30.4	3.97
5	1.82	2.51	94.9	-30.7	7.41
6	1.81	2.50	94.8	-32.2	5.93
7	1.77	2.44	94.8	-35.0	4.47
8	1.75	2.41	94.7	-	3.83
9	1.79	2.46	94.8	-26.3	4.76
10	1.78	2.45	94.8	-33.4	3.78
Mean	1.794	2.471	94.8	-31.7	4.78
SD	0.026	0.036	0.001	2.56	1.25

Five grouped elements

Pattern no.	-3 dB beam width [mm]	-6 dB beam width [mm]	Remaining intensity [%]	Average side lobe level [dB]	Noise floor increase [ΔdB]
Intact	1.79	2.46	-	-	-
1	1.74	2.38	94.8	-14.3	0.40
2	1.78	2.46	94.7	-18.7	2.63
3	1.79	2.46	94.8	-	5.15
4	1.78	2.45	94.9	-18.7	0.35
5	1.76	2.42	94.8	-	0.43
6	1.77	2.43	94.8	-	4.96
7	1.76	2.42	94.8	-35.0	5.08
8	1.81	2.51	94.9	-21.6	4.40
9	1.76	2.42	94.7	-14.8	3.78
10	1.76	2.43	94.8	-30.0	4.84
Mean	1.77	2.44	94.8	-21.9	3.20
SD	0.02	0.03	0.001	7.81	2.08

Five edge elements

Pattern no.	-3 dB beam width [mm]	-6 dB beam width [mm]	Remaining intensity [%]	Average side lobe level [dB]	Noise floor increase [ΔdB]
Intact	1.79	2.46	-	-	-
1	1.88	2.58	95.0	-	0.34
2	1.88	2.58	95.0	-	0.34
3	1.89	2.60	94.7	-	0.43
4	1.88	2.58	95.0	-	0.34
5	1.88	2.58	94.9	-	0.36
6	1.89	2.60	94.7	-	0.43
7	1.89	2.60	94.8	-	0.41
8	1.88	2.60	94.8	-	0.39
9	1.88	2.58	95.0	-	0.34
10	1.89	2.60	94.7	-	0.43
Mean	1.88	2.59	94.9	-	0.38
SD	0.01	0.01	0.001	-	0.04

Ten random elements

Pattern no.	-3 dB beam width [mm]	-6 dB beam width [mm]	Remaining intensity [%]	Average side lobe level [dB]	Noise floor increase [ΔdB]
Intact	1.79	2.46	-	-	-
1	1.85	2.56	89.5	-26.0	4.23
2	1.85	2.55	89.5	-24.1	4.25
3	1.80	2.48	89.5	-30.0	6.39
4	1.81	2.50	89.7	-30.2	7.87
5	1.74	2.40	89.5	-32.9	5.99
6	1.78	2.45	89.6	-33.0	5.15
7	1.81	2.50	89.5	-	5.73
8	1.76	2.42	89.6	-29.6	5.51
9	1.80	2.48	89.6	-27.2	4.54
10	1.77	2.42	89.7	-25.5	5.13
Mean	1.80	2.48	89.6	-28.7	5.48
SD	0.04	0.05	0.001	3.19	1.11

Ten grouped elements

Pattern no.	-3 dB beam width [mm]	-6 dB beam width [mm]	Remaining intensity [%]	Average side lobe level [dB]	Noise floor increase [ΔdB]
Intact	1.79	2.46	-	-	-
1	1.74	2.39	89.6	-13.7	4.65
2	1.97	2.72	89.7	-28.5	5.78
3	1.85	2.59	89.3	-17.3	0.93
4	1.86	2.57	89.6	-22.1	4.45
5	1.75	2.42	89.7	-15.2	0.75
6	1.82	2.52	89.4	-18.3	5.16
7	1.81	2.50	89.7	-19.5	3.58
8	1.80	2.48	89.4	-22.3	4.59
9	1.70	2.32	89.6	-12.9	7.23
10	1.81	2.51	89.8	-19.1	4.57
Mean	1.81	2.50	89.6	-18.9	4.17
SD	0.075	0.11	0.002	4.63	2.00

Ten edge elements

Pattern no.	-3 dB beam width [mm]	-6 dB beam width [mm]	Remaining intensity [%]	Average side lobe level [dB]	Noise floor increase [ΔdB]
Intact	1.79	2.46		-	-
1	1.98	2.72	89.9	-	0.70
2	2.00	2.74	89.6	-	0.82
3	1.98	2.73	89.9	-	0.72
4	2.01	2.76	89.4	-	0.88
5	2.00	2.74	89.6	-	0.82
6	1.98	2.72	89.9	-	0.70
7	1.98	2.73	89.8	-	0.75
8	2.02	2.77	89.3	-	0.93
9	1.99	2.74	89.7	-	0.77
10	2.01	2.77	89.3	-	0.90
Mean	1.99	2.74	89.7	-	0.80
SD	0.01	0.02	0.002	-	0.08

Fifteen random elements

Pattern no.	-3 dB beam width [mm]	-6 dB beam width [mm]	Remaining intensity [%]	Average side lobe level [dB]	Noise floor increase [ΔdB]
Intact	1.79	2.46	-	-	-
1	1.88	2.60	84.3	-23.1	4.76
2	1.82	2.52	84.3	-29.8	6.88
3	1.80	2.47	84.4	-29.7	8.37
4	1.76	2.42	84.4	-29.8	5.61
5	1.80	2.47	84.3	-21.5	7.05
6	1.80	2.48	84.4	-26.8	5.44
7	1.77	2.43	84.4	-28.7	6.36
8	1.85	2.55	84.4	-22.1	7.11
9	1.78	2.45	84.4	-24.0	5.74
10	1.79	2.46	84.5	-28.2	6.55
Mean	1.80	2.49	84.4	-26.4	6.39
SD	0.04	0.05	0.001	3.38	1.04

Fifteen grouped elements

Pattern no.	-3 dB beam width [mm]	-6 dB beam width [mm]	Remaining intensity [%]	Average side lobe level [dB]	Noise floor increase [ΔdB]
Intact	1.79	2.46		-	-
1	1.84	2.56	84.6	-15.5	4.77
2	1.78	2.46	84.5	-14.7	6.08
3	1.71	2.37	84.5	-12.8	1.19
4	1.69	2.35	84.2	-12.7	3.71
5	1.86	2.60	84.1	-18.8	1.42
6	1.65	2.25	84.3	-11.0	5.92
7	1.78	2.46	84.2	-18.5	4.05
8	1.82	2.53	84.6	-16.5	1.26
9	1.80	2.46	84.6	-13.2	5.82
10	1.78	2.46	84.6	-16.2	5.44
Mean	1.77	2.45	84.4	-15.0	3.97
SD	0.07	0.10	0.002	2.60	2.00

Twenty random elements

Pattern no.	-3 dB beam width [mm]	-6 dB beam width [mm]	Remaining intensity [%]	Average side lobe level [dB]	Noise floor increase [ΔdB]
Intact	1.79	2.46	-	-	-
1	1.91	2.65	79.0	-24.0	7.32
2	1.78	2.46	79.2	-16.8	8.88
3	1.74	2.39	79.2	-21.6	6.54
4	1.76	2.42	79.1	-25.8	7.40
5	1.76	2.43	79.2	-26.0	6.87
6	1.89	2.61	79.2	-21.7	7.69
7	1.77	2.43	79.2	-24.4	6.38
8	1.87	2.59	79.3	-24.9	8.46
9	1.69	2.31	79.2	-27.7	7.00
10	1.74	2.40	79.1	-19.3	7.17
Mean	1.79	2.47	79.2	-23.2	7.37
SD	0.07	0.11	0.001	3.34	0.79

Twenty grouped elements

Pattern no.	-3 dB beam width [mm]	-6 dB beam width [mm]	Remaining intensity [%]	Average side lobe level [dB]	Noise floor increase [ΔdB]
Intact	1.79	2.46	-	-	-
1	1.95	2.73	79.5	-17.2	5.75
2	1.76	2.41	79.1	-19.5	6.85
3	1.85	2.55	79.4	-21.1	6.53
4	1.74	2.46	78.9	-18.7	1.92
5	1.75	2.42	79.1	-13.5	5.61
6	1.80	2.57	79.5	-13.7	6.28
7	1.91	2.65	79.3	-18.6	4.18
8	1.59	2.17	79.1	-9.09	1.83
9	1.73	2.41	79.1	-12.8	7.37
10	1.76	2.48	79.4	-14.6	1.57
Mean	1.79	2.48	79.2	-15.9	4.79
SD	0.10	0.15	0.002	3.73	2.25

Thirty random elements

Pattern no.	-3 dB beam width [mm]	-6 dB beam width [mm]	Remaining intensity [%]	Average side lobe level [dB]	Noise floor increase [ΔdB]
Intact	1.79	2.46	-	-	-
1	1.91	2.66	68.7	-23.3	10.1
2	1.80	2.48	68.7	-20.1	8.41
3	1.72	2.36	68.8	-24.9	9.38
4	1.85	2.56	68.8	-19.7	8.89
5	1.80	2.48	68.9	-27.6	9.66
6	1.66	2.28	68.7	-23.9	9.37
7	1.80	2.50	68.8	-20.5	8.59
8	1.81	2.50	68.7	-23.6	10.3
9	1.78	2.46	68.7	-22.4	9.68
10	1.79	2.46	68.8	-25.4	8.16
Mean	1.79	2.47	68.8	-23.2	9.25
SD	0.07	0.10	0.001	2.52	0.71

Thirty grouped elements

Pattern no.	-3 dB beam width [mm]	-6 dB beam width [mm]	Remaining intensity [%]	Average side lobe level [dB]	Noise floor increase [ΔdB]
Intact	1.79	2.46	-	-	-
1	1.57	2.14	68.7	-9.15	2.93
2	1.71	2.36	68.5	-9.34	6.88
3	2.23	3.10	68.2	-14.0	8.69
4	1.68	2.34	68.9	-12.7	5.80
5	1.82	2.65	69.2	-17.7	6.62
6	1.76	2.47	68.5	-11.9	8.76
7	1.65	2.30	68.5	-11.6	7.82
8	1.73	2.46	69.0	-18.3	5.90
9	1.65	2.25	68.8	-10.8	5.32
10	1.65	2.25	68.8	-11.1	5.82
Mean	1.74	2.43	68.7	-12.6	6.45
SD	0.19	0.28	0.003	3.14	1.74

Appendix 5

Below are the total results from Test I with forty degree steering. The measurements are taken at a depth of 7.76 cm. The noise floor for the intact transducer is -36.1 dB, the values given under “Noise floor increase” are the deviations from this value.

Five random elements

Pattern no.	-3 dB beam width [mm]	-6 dB beam width [mm]	Remaining intensity [%]	Average side lobe level [dB]	Noise floor increase [ΔdB]
Intact	2.20	3.04	-	-	-
1	2.24	3.09	94.7	-16.3	1.51
2	2.24	3.09	94.7	-31.8	2.42
3	2.22	3.08	94.7	-30.1	-0.03
4	2.18	3.01	94.8	-29.8	2.61
5	2.23	3.09	94.9	-29.4	1.37
6	2.23	3.08	94.8	-31.2	2.67
7	2.18	3.01	94.8	-34.1	0.39
8	2.16	2.97	94.7	-33.8	0.43
9	2.19	3.02	94.9	-26.3	0.34
10	2.19	3.01	94.8	-32.2	2.26
Mean	2.21	3.04	94.8	-29.5	1.40
SD	0.03	0.04	0.001	5.18	1.05

Five grouped elements

Pattern no.	-3 dB beam width [mm]	-6 dB beam width [mm]	Remaining intensity [%]	Average side lobe level [dB]	Noise floor increase [ΔdB]
Intact	2.20	3.04	-	-	-
1	2.14	2.94	94.8	-14.5	2.73
2	2.19	3.03	94.7	-20.0	2.76
3	2.20	3.02	94.8	-23.4	2.97
4	2.18	3.01	94.9	-18.7	4.02
5	2.16	2.98	94.7	-	0.95
6	2.18	2.99	94.8	-	3.74
7	2.16	2.99	94.7	-34.0	2.57
8	2.23	3.08	95.0	-21.6	4.49
9	2.17	2.98	94.7	-14.6	3.99
10	2.17	2.98	94.8	-29.5	2.75
Mean	2.18	3.00	94.8	-22.0	3.10
SD	0.03	0.04	0.001	6.86	1.02

Five edge elements

Pattern no.	-3 dB beam width [mm]	-6 dB beam width [mm]	Remaining intensity [%]	Average side lobe level [dB]	Noise floor increase [ΔdB]
Intact	2.20	3.04	-	-	-
1	2.30	3.17	95.1	-	0.29
2	2.30	3.17	95.1	-	0.29
3	2.33	3.22	94.6	-	0.42
4	2.30	3.17	95.1	-	0.29
5	2.31	3.18	95.0	-	0.33
6	2.33	3.22	94.6	-	0.42
7	2.32	3.20	94.8	-	0.39
8	2.32	3.20	94.9	-	0.36
9	2.30	3.17	95.1	-	0.29
10	2.33	3.22	94.6	-	0.42
Mean	2.32	3.19	94.9	-	0.35
SD	0.02	0.02	0.002	-	0.06

Ten random elements

Pattern no.	-3 dB beam width [mm]	-6 dB beam width [mm]	Remaining intensity [%]	Average side lobe level [dB]	Noise floor increase [ΔdB]
Intact	2.20	3.04	-	-	-
1	2.28	3.16	89.5	-26.0	5.75
2	2.28	3.14	89.4	-24.1	5.70
3	2.21	3.06	89.5	-29.7	3.32
4	2.23	3.07	89.7	-29.0	3.11
5	2.14	2.96	89.5	-31.4	0.83
6	2.19	3.01	89.6	-31.8	2.68
7	2.22	3.07	89.5	-	3.55
8	2.16	2.97	89.6	-29.3	3.07
9	2.22	3.06	89.6	-26.9	5.51
10	2.17	2.98	89.7	-25.5	-0.33
Mean	2.21	3.05	89.6	-28.2	3.32
SD	0.05	0.07	0.001	2.68	2.01

Ten grouped elements

Pattern no.	-3 dB beam width [mm]	-6 dB beam width [mm]	Remaining intensity [%]	Average side lobe level [dB]	Noise floor increase [ΔdB]
Intact	2.20	3.04	-	-	-
1	2.14	2.94	89.7	-13.3	6.44
2	2.42	3.33	89.8	-27.7	6.52
3	2.28	3.21	89.3	-17.1	0.91
4	2.28	3.16	89.6	-21.9	5.96
5	2.15	2.97	89.8	-15.2	0.73
6	2.23	3.12	89.3	-18.1	3.27
7	2.23	3.08	89.8	-19.5	4.47
8	2.20	3.06	89.4	-21.4	4.48
9	2.09	2.86	89.6	-13.0	2.63
10	2.23	3.08	89.9	-19.0	6.36
Mean	2.22	3.08	89.6	-18.6	4.18
SD	0.09	0.14	0.002	4.42	2.22

Ten edge elements

Pattern no.	-3 dB beam width [mm]	-6 dB beam width [mm]	Remaining intensity [%]	Average side lobe level [dB]	Noise floor increase [ΔdB]
Intact	2.20	3.04	-	-	-
1	2.41	3.32	90.1	-	0.62
2	2.46	3.38	89.6	-	0.77
3	2.42	3.33	90.0	-	0.65
4	2.48	3.42	89.3	-	0.86
5	2.46	3.38	89.6	-	0.77
6	2.41	3.32	90.1	-	0.62
7	2.43	3.35	89.9	-	0.68
8	2.50	3.45	89.1	-	0.93
9	2.43	3.37	89.8	-	0.71
10	2.50	3.43	89.2	-	0.89
Mean	2.22	3.06	89.7	-	0.75
SD	0.05	0.07	0.004	-	0.12

Fifteen random elements

Pattern no.	-3 dB beam width [mm]	-6 dB beam width [mm]	Remaining intensity [%]	Average side lobe level [dB]	Noise floor increase [ΔdB]
Intact	2.20	3.04	-	-	-
1	2.31	3.20	84.2	-23.1	6.49
2	2.24	3.12	84.2	-29.5	3.00
3	2.20	3.04	84.4	-28.4	3.54
4	2.16	2.98	84.4	-21.2	3.96
5	2.21	3.06	84.3	-21.5	4.55
6	2.21	3.04	84.5	-25.5	3.75
7	2.17	2.99	84.4	-29.0	4.50
8	2.28	3.15	84.4	-21.8	6.30
9	2.19	3.01	84.5	-23.6	3.29
10	2.20	3.02	84.5	-27.9	5.00
Mean	2.22	3.06	84.4	-25.2	4.44
SD	0.05	0.07	0.001	3.33	1.20

Fifteen grouped elements

Pattern no.	-3 dB beam width [mm]	-6 dB beam width [mm]	Remaining intensity [%]	Average side lobe level [dB]	Noise floor increase [ΔdB]
Intact	2.20	3.04	-	-	-
1	2.25	3.14	84.7	-15.6	3.64
2	2.19	3.03	84.5	-14.8	5.24
3	2.11	2.92	84.7	-13.1	1.16
4	2.08	2.90	84.1	-11.9	1.35
5	2.30	3.23	83.9	-18.4	2.97
6	2.03	2.77	84.4	-11.0	3.82
7	2.18	3.03	84.2	-16.4	4.21
8	2.23	3.09	84.8	-16.6	4.97
9	2.20	3.02	84.7	-13.3	4.68
10	2.18	3.02	84.7	-16.3	4.53
Mean	2.18	3.02	84.5	-14.7	3.66
SD	0.08	0.13	0.003	2.37	1.43

Twenty random elements

Pattern no.	-3 dB beam width [mm]	-6 dB beam width [mm]	Remaining intensity [%]	Average side lobe level [dB]	Noise floor increase [ΔdB]
Intact	2.20	3.04	-	-	-
1	2.36	3.27	79.0	-24.0	4.91
2	2.19	3.02	79.2	-16.7	6.03
3	2.14	2.94	79.2	-21.5	5.24
4	2.17	2.98	79.1	-25.5	6.43
5	2.17	2.98	79.2	-25.8	2.54
6	2.32	3.21	79.2	-21.4	6.74
7	2.18	2.99	79.3	-15.4	5.10
8	2.30	3.18	79.4	-24.6	6.24
9	2.07	2.84	79.2	-13.9	5.78
10	2.14	2.96	79.1	-19.3	4.48
Mean	2.20	3.04	79.2	-20.8	5.35
SD	0.09	0.14	0.001	4.32	1.22

Twenty grouped elements

Pattern no.	-3 dB beam width [mm]	-6 dB beam width [mm]	Remaining intensity [%]	Average side lobe level [dB]	Noise floor increase [ΔdB]
Intact	2.20	3.04	-	-	-
1	2.39	3.33	79.6	-17.2	7.32
2	2.17	2.98	79.0	-12.1	7.55
3	2.26	3.11	79.5	-14.2	6.05
4	2.14	3.04	78.7	-18.6	2.40
5	2.16	2.98	79.0	-13.4	6.65
6	2.22	3.14	79.7	-13.8	6.90
7	2.34	3.25	79.3	-18.4	5.65
8	1.96	2.68	79.0	-9.02	2.35
9	2.12	2.96	79.1	-28.2	4.37
10	2.16	3.03	79.6	-14.7	1.56
Mean	2.19	3.05	79.3	-16.0	5.08
SD	0.12	0.18	0.003	5.20	2.25

Thirty random elements

Pattern no.	-3 dB beam width [mm]	-6 dB beam width [mm]	Remaining intensity [%]	Average side lobe level [dB]	Noise floor increase [ΔdB]
Intact	2.20	3.04	-	-	-
1	2.36	3.30	68.5	-23.3	6.78
2	2.20	3.06	68.7	-20.1	5.72
3	2.11	2.90	68.8	-20.5	5.39
4	2.28	3.15	68.9	-19.4	6.29
5	2.20	3.03	69.0	-27.4	7.37
6	2.04	2.80	68.7	-13.2	6.77
7	2.22	3.06	68.9	-20.5	7.59
8	2.23	3.09	68.6	-23.4	5.79
9	2.18	3.03	68.7	-13.1	6.60
10	2.20	3.02	68.8	-25.3	3.07
Mean	2.20	3.04	68.8	-20.6	6.14
SD	0.09	0.13	0.00	4.66	1.29

Thirty grouped elements

Pattern no.	-3 dB beam width [mm]	-6 dB beam width [mm]	Remaining intensity [%]	Average side lobe level [dB]	Noise floor increase [ΔdB]
Intact	2.20	3.04	-	-	-
1	1.93	2.64	68.6	-9.36	6.52
2	2.10	2.92	68.4	-9.20	3.09
3	2.79	3.89	68.0	-13.7	5.67
4	2.07	2.88	69.1	-12.9	6.82
5	2.24	3.22	69.4	-13.8	5.30
6	2.17	3.07	68.3	-25.6	7.54
7	2.03	2.86	68.4	-11.5	6.31
8	2.13	3.01	69.2	-18.3	6.20
9	2.02	2.77	68.8	-10.8	2.76
10	2.02	2.76	68.9	-11.2	6.54
Mean	2.15	3.00	68.7	-13.6	5.68
SD	0.24	0.35	0.004	4.96	1.57

Appendix 6

The results from Test II are presented below. All measures, but the intensity in the cyst, were taken at a depth of 7.76 cm in a point spreader. The cyst was located at a depth of 5.81 cm.

Five random elements

Pattern no.	-6dB beam width [mm]	-12dB beam width [mm]	SNR[dB]	Remaining peak intensity [%]	Remaining cyst intensity [%]
Intact	1.64	2.19	35.5	-	-
1	1.67	2.22	35.8	94.9	95.1
2	1.67	2.22	35.9	94.5	94.7
3	1.67	2.22	36.5	95.0	95.1
4	1.63	2.18	35.8	94.9	94.7
5	1.67	2.23	36.5	94.8	95.0
6	1.66	2.21	36.1	94.9	95.0
7	1.63	2.17	35.2	94.7	94.5
8	1.61	2.15	34.4	94.9	94.8
9	1.64	2.19	36.3	94.9	94.9
10	1.63	2.17	34.3	94.8	94.8
Mean	1.65	2.20	35.7	94.8	94.9
SD	0.02	0.03	0.79	0.00	0.00

Five grouped elements

Pattern no.	-6dB beam width [mm]	-12dB beam width [mm]	SNR[dB]	Remaining peak intensity [%]	Remaining cyst intensity [%]
Intact	1.64	2.19	35.5	-	-
1	1.58	2.12	32.0	94.7	94.7
2	1.65	2.19	36.3	94.8	94.8
3	1.64	2.20	36.4	94.8	94.5
4	1.63	2.18	34.4	94.3	94.3
5	1.62	2.16	35.1	95.2	95.2
6	1.63	2.17	35.8	94.8	94.8
7	1.62	2.17	35.4	95.2	95.2
8	1.67	2.24	37.1	94.7	94.3
9	1.61	2.15	33.1	94.8	94.8
10	1.61	2.16	34.6	94.8	94.1
Mean	1.63	2.17	35.0	94.8	94.7
SD	0.03	0.03	1.56	0.00	0.00

Five edge elements

Pattern no.	-6dB beam width [mm]	-12dB beam width [mm]	SNR[dB]	Remaining peak intensity [%]	Remaining cyst intensity [%]
Intact	1.64	2.19	35.5	-	-
1	1.70	2.27	36.6	95.3	95.4
2	1.70	2.27	36.6	95.3	95.4
3	1.71	2.26	35.6	95.4	95.8
4	1.70	2.27	36.6	95.3	95.4
5	1.70	2.26	36.4	95.6	95.8
6	1.71	2.26	35.6	95.4	95.8
7	1.70	2.26	35.9	95.6	95.9
8	1.70	2.26	36.1	95.7	95.8
9	1.70	2.27	36.6	95.3	95.4
10	1.71	2.26	35.6	95.4	95.8
Mean	1.70	2.26	36.2	95.4	95.6
SD	0.00	0.00	0.42	0.00	0.00

Ten random elements

Pattern no.	-6dB beam width [mm]	-12dB beam width [mm]	SNR[dB]	Remaining peak intensity [%]	Remaining cyst intensity [%]
Intact	1.64	2.19	35.5	-	-
1	1.70	2.25	36.6	89.5	90.0
2	1.69	2.24	35.8	89.5	89.9
3	1.66	2.21	36.9	89.9	89.8
4	1.66	2.21	35.5	89.4	89.6
5	1.61	2.15	35.4	89.9	89.7
6	1.63	2.19	35.5	89.5	89.5
7	1.67	2.22	36.6	89.0	89.1
8	1.61	2.16	34.3	89.5	89.3
9	1.66	2.21	35.6	89.5	89.5
10	1.61	2.16	34.2	89.4	89.3
Mean	1.65	2.20	35.6	89.5	89.6
SD	0.03	0.04	0.90	0.00	0.00

Ten grouped elements

Pattern no.	-6dB beam width [mm]	-12dB beam width [mm]	SNR[dB]	Remaining peak intensity [%]	Remaining cyst intensity [%]
Intact	1.64	2.19	35.5	-	-
1	1.59	2.13	32.6	89.1	89.1
2	1.77	2.34	37.2	90.0	90.5
3	1.72	2.27	38.7	89.4	89.3
4	1.72	2.27	38.4	89.1	89.5
5	1.59	2.14	31.0	88.5	88.5
6	1.68	2.23	37.4	89.1	89.0
7	1.66	2.23	35.1	88.7	88.7
8	1.67	2.22	36.4	90.4	90.6
9	1.52	2.06	29.1	89.2	88.8
10	1.67	2.24	35.0	88.6	88.8
Mean	1.66	2.21	35.1	89.2	89.3
SD	0.07	0.08	3.23	0.01	0,01

Ten edge elements

Pattern no.	-6dB beam width [mm]	-12dB beam width [mm]	SNR[dB]	Remaining peak intensity [%]	Remaining cyst intensity [%]
Intact	1.64	2.19	35.5	-	-
1	1.77	2.36	37.5	90.1	90.3
2	1.77	2.34	36.6	90.6	91.2
3	1.77	2.35	37.4	90.5	90.7
4	1.78	2.34	35.9	90.2	91.1
5	1.77	2.34	36.6	90.6	91.2
6	1.77	2.36	37.5	90.1	90.3
7	1.77	2.34	37.2	90.7	90.9
8	1.79	2.34	35.5	89.7	90.7
9	1.77	2.34	37.0	90.6	91.0
10	1.78	2.34	35.6	90.0	90.9
Mean	1.77	2.34	36.7	90.3	90.8
SD	0.01	0.01	0.77	0.00	0.00

Fifteen random elements

Pattern no.	-6dB beam width [mm]	-12dB beam width [mm]	SNR[dB]	Remaining peak intensity [%]	Remaining cyst intensity [%]
Intact	1.64	2.19	35.4	-	-
1	1.73	2.28	37.0	84.3	84.8
2	1.68	2.23	37.1	84.3	84.5
3	1.65	2.20	36.2	84.5	84.6
4	1.62	2.17	35.3	84.3	84.4
5	1.66	2.21	36.1	84.0	84.0
6	1.64	2.19	34.4	84.2	84.2
7	1.63	2.19	36.9	84.2	84.0
8	1.69	2.24	36.2	84.3	84.4
9	1.63	2.19	35.4	84.4	84.1
10	1.63	2.19	33.3	83.7	83.9
Mean	1.66	2.21	35.8	84.2	84.3
SD	0.03	0.03	1.22	0.00	0.00

Fifteen grouped elements

Pattern no.	-6dB beam width [mm]	-12dB beam width [mm]	SNR[dB]	Remaining peak intensity [%]	Remaining cyst intensity [%]
Intact	1.64	2.19	35.5	-	-
1	1.68	2.28	35.9	83.9	78.3
2	1.62	2.18	31.3	83.2	77.7
3	1.55	2.09	27.0	83.2	77.6
4	1.57	2.10	32.4	86.2	80.4
5	1.73	2.28	36.6	83.6	78.0
6	1.45	1.99	26.9	84.2	78.6
7	1.64	2.18	35.4	83.6	78.0
8	1.67	2.27	37.0	84.4	78.8
9	1.62	2.17	31.4	84.8	79.1
10	1.63	2.22	35.7	84.2	78.6
Mean	1.62	2.18	33.0	84.1	78.5
SD	0.08	0.09	3.78	0.01	0.01

Twenty random elements

Pattern no.	-6dB beam width [mm]	-12dB beam width [mm]	SNR[dB]	Remaining peak intensity [%]	Remaining cyst intensity [%]
Intact	1.64	2.19	35.5	-	-
1	1.75	2.31	37.3	80.0	79.6
2	1.65	2.20	37.2	79.4	79.3
3	1.60	2.14	34.8	78.9	78.8
4	1.62	2.17	34.8	78.9	78.7
5	1.62	2.17	35.6	79.0	79.1
6	1.72	2.28	37.5	78.8	79.0
7	1.61	2.17	33.2	79.1	78.9
8	1.71	2.28	37.1	79.2	79.3
9	1.52	2.07	31.1	79.2	78.8
10	1.60	2.16	35.4	79.5	78.8
Mean	1.64	2.19	35.4	79.1	79.0
SD	0.07	0.07	2.06	0.00	0.00

Twenty grouped elements

Pattern no.	-6dB beam width [mm]	-12dB beam width [mm]	SNR[dB]	Remaining peak intensity [%]	Remaining cyst intensity [%]
Intact	1.64	2.19	35.5	-	-
1	1.76	2.37	35.3	78.5	73.2
2	1.59	2.13	31.4	80.0	74.7
3	1.69	2.26	36.5	79.0	73.6
4	1.62	2.16	32.5	79.3	74.0
5	1.61	2.16	33.1	78.6	73.3
6	1.65	2.26	29.0	78.1	72.9
7	1.75	2.32	39.0	78.4	73.2
8	1.38	1.95	23.8	79.0	73.8
9	1.60	2.14	33.3	80.4	75.1
10	1.60	2.19	28.0	78.0	72.8
Mean	1.63	2.19	32.2	78.9	73.7
SD	0.10	0.12	4.41	0.01	0.01

Thirty random elements

Pattern no.	-6dB beam width [mm]	-12dB beam width [mm]	SNR[dB]	Remaining peak intensity [%]	Remaining cyst intensity [%]
Intact	1.64	2.19	35.5	-	-
1	1.76	2.31	38.7	68.7	69.2
2	1.66	2.22	37.7	68.3	68.4
3	1.57	2.11	33.9	68.7	68.4
4	1.70	2.26	37.0	68.7	68.6
5	1.63	2.19	33.4	68.5	68.4
6	1.49	2.04	30.0	68.9	68.4
7	1.65	2.22	33.3	67.5	67.5
8	1.68	2.22	36.0	68.8	69.1
9	1.65	2.21	34.9	69.6	69.4
10	1.63	2.17	33.0	68.6	68.6
Mean	1.64	2.20	34.8	68.6	68.6
SD	0.07	0.07	2.60	0.01	0.01

Thirty grouped elements

Pattern no.	-6dB beam width [mm]	-12dB beam width [mm]	SNR[dB]	Remaining peak intensity [%]	Remaining cyst intensity [%]
Intact	1.64	2.19	35.5	-	-
1	1.35	1.92	22.4	68.3	67.7
2	1.55	2.08	26.2	67.5	67.3
3	1.89	2.47	35.4	68.1	69.2
4	1.54	2.13	29.2	69.9	69.1
5	1.68	2.28	25.9	66.6	66.6
6	1.62	2.15	31.7	70.7	71.2
7	1.52	2.04	31.4	68.3	68.1
8	1.59	2.18	25.7	68.2	67.8
9	1.51	2.04	34.7	68.8	68.6
10	1.45	2.01	27.5	68.4	68.0
Mean	1.57	2.13	29.0	68.5	68.3
SD	0.14	0.16	4.24	0.01	0.01